

Geochronology of igneous rocks in the Sierra Norte de Córdoba (Argentina): Implications for the Pampean evolution at the western Gondwana margin

W. von Gosen^{1,*}, W.C. McClelland^{2,*}, W. Loske^{3,*}, J.C. Martínez^{4,5,*}, and C. Prozzi^{4,*}

¹GEOTRUM NORDBAYERN, KRUSTENDYNAMIK, FRIEDRICH-ALEXANDER-UNIVERSITÄT ERLANGEN-NÜRNBERG, SCHLOSSGARTEN 5, D-91054 ERLANGEN, GERMANY

²DEPARTMENT OF EARTH AND ENVIRONMENTAL SCIENCES, UNIVERSITY OF IOWA, 121 TROWBRIDGE HALL, IOWA CITY, IOWA 52242, USA

³DEPARTMENT FÜR GEO- UND UMWELTWISSENSCHAFTEN, SEKTION GEOLOGIE, LUDWIG-MAXIMILIANS-UNIVERSITÄT MÜNCHEN, LUISENSTRASSE 37, D-80333 MÜNCHEN, GERMANY

⁴DEPARTAMENTO DE GEOLOGÍA, UNIVERSIDAD NACIONAL DEL SUR, SAN JUAN 670, 8000 BAHÍA BLANCA, ARGENTINA

⁵INGEOSUR-CONICET

ABSTRACT

U-Pb zircon data (secondary ion mass spectrometry [SIMS] and thermal ionization mass spectrometry [TIMS] analyses) from igneous rocks with differing structural fabrics in the Sierra Norte de Córdoba, western Argentina, suggest that the sedimentary, tectonic, and magmatic history in this part of the Eastern Sierras Pampeanas spans the late Neoproterozoic–Early Cambrian. A deformed metarhyolite layer in metaclastic sedimentary rocks gives a crystallization age of 535 ± 5 Ma, providing a limit on the timing of the onset of D_1 deformation and metamorphism. The new data coupled with published Neoproterozoic zircon dates from a rhyolite beneath the metaclastic section and detrital zircon ages from the section indicate a late Neoproterozoic to Early Cambrian depositional age, making this section time equivalent with the Puncoviscana Formation (*sensu lato*) of northwest Argentina. A synkinematic granite porphyry gives a crystallization age of 534 ± 5 Ma, providing a limit on the age of dextral mylonitization in the Sierra Norte area (D_2 event). The new age is consistent with ages of 533 ± 4 Ma from a mylonitic granite with dextral sense-of-shear fabrics and 531 ± 4 Ma from a late-synkinematic dacitic porphyry, which broadly indicates the final age of dextral deformation. A crystallization age of zircons from the postkinematic, high-level El Tío granite (530 ± 4 Ma) suggests that both stages of Pampean deformation and regional metamorphism, accompanied by synkinematic intrusions, were followed by uplift and took place during a very short time span in the Early Cambrian. This is supported by zircon dates of 523 ± 5 Ma from a rhyolite to dacite in the western part of the Rodeito area and dates from the undeformed El Escondido rhyolite and granite of 519 ± 4 Ma and 521 ± 4 Ma, respectively. These three crystallization ages also indicate that ductile dextral shearing and mylonitization associated with the Pampean D_2 event terminated in the Early Cambrian. Both stages of Pampean deformation in this segment of the western pre-Andean Gondwana margin seem to represent a continuous event that can be related to oblique dextral convergence between the overriding plate in the east and the subducting and finally colliding plate in the west. The postkinematic intrusions and extrusions are related to the late stage of the Pampean magmatic history, which terminated before Early Ordovician (Famatinian) time.

LITHOSPHERE, v. 6; no. 4; p. 277–300; GSA Data Repository Item 2014169 | Published online 12 May 2014

doi: 10.1130/L344.1

INTRODUCTION

The tectonic history of the Eastern Sierras Pampeanas metamorphic complex in western Argentina (Fig. 1) has been interpreted in two fundamentally different ways. The first set of models interprets the complex as a continental terrane. This crustal fragment was referred to as the allochthonous Pampean terrane (Ramos, 1988) or “Pampia” (e.g., Ramos, 1999; Ramos et al., 2010), which collided with the western margin of Gondwana in Early Cambrian time (e.g., Rapela et al., 1998a, 2001; Baldo et al., 1999) along a collision zone exposed in the Sierras de Córdoba in the easternmost part of the East-

ern Sierras Pampeanas (Fig. 1). The interpretation of the Pampean terrane as a fragment of the autochthonous Río de la Plata craton that rifted from the margin and subsequently collided again (Rapela et al., 1998a, 2001; von Gosen et al., 2002) has been excluded by the models of Rapela et al. (2007) and Casquet et al. (2012). Pampia has more recently been interpreted as a cratonic fragment of Rodinia that collided with the Río de la Plata craton in the east (Ramos et al., 2010, with references therein). As an alternative, it has been proposed that the continental terrane, named MARA (Casquet et al., 2012), consists of basement of Mesoproterozoic or “Grenville” age and represents the Western Sierras Pampeanas (Rapela et al., 2007; Casquet et al., 2012). In this interpretation, the terrane collided with the Eastern Sierras Pampeanas during the Pampean orogeny (Casquet et al., 2012;

Iannizzotto et al., 2013). Similar models have been proposed by Siegesmund et al. (2010) and Escayola et al. (2011).

A second set of models suggests that contractional deformation, metamorphism, and magmatism recorded in the Eastern Sierras Pampeanas metamorphic complex resulted from ridge subduction and subsequent ridge collision (Simpson et al., 2003; Gromet et al., 2005; Schwartz et al., 2008). Models that do not invoke collision of a continental fragment (Simpson et al., 2003; Whitmeyer and Simpson, 2004; Schwartz et al., 2008) are supported by the lack of clear basement rocks of the Río de la Plata craton exposed in the Sierras de Córdoba. Paleoproterozoic zircon ages from drill cores in the central and southeastern Córdoba Province, east of the Sierras de Córdoba, provide the first definitive evidence for the western extent of the Río de la Plata cra-

*werner.von.gosen@fau.de; bill-mcclelland@uiowa.edu; wloske@iaag.geo.uni-muenchen.de; jcmartin@uns.edu.ar; cprozzi@gmail.com.

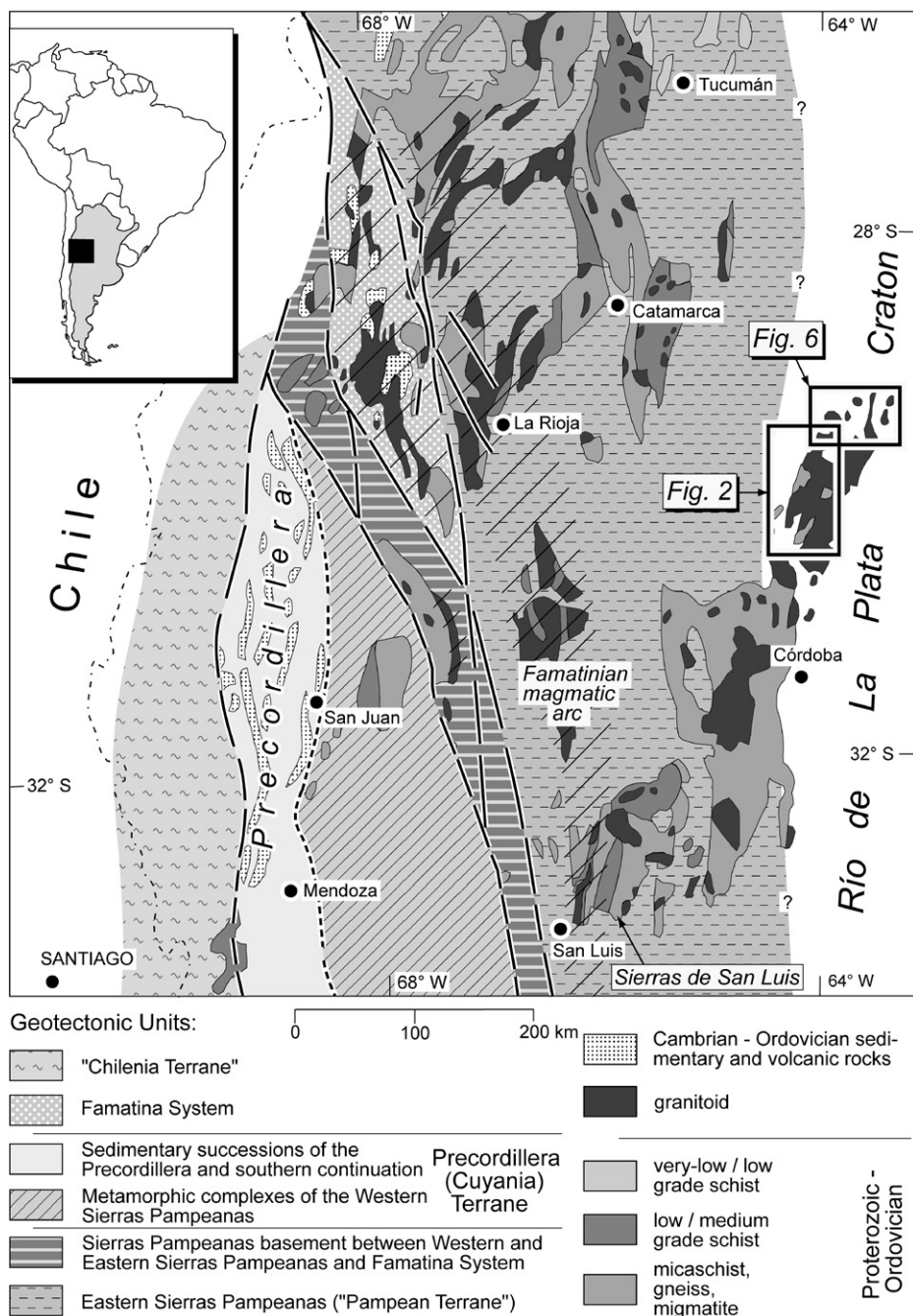


Figure 1. Geological map of the northwestern Argentine Andes showing main geotectonic units (modified from von Gosen and Prozzi, 2009; and information in Verdecchia et al., 2007; de los Hoyos et al., 2011; Larrovere et al., 2011). Frames show locations of maps of Figures 2 and 6 in the Sierra Norte de Córdoba and southern part of the Santiago del Estero Province.

tonic basement (Rapela et al., 2005, 2007). East- or northeast-directed subduction led to widespread arc-related magmatism and formation of an accretionary prism in the western portion of the complex (e.g., Northrup et al., 1998; Rapela et al., 1998a), all of which were accreted to the western Gondwana margin during contractional Pampean deformation (e.g., Piñán-Llamas and Simpson, 2006; Steenken et al., 2011).

Schwartz and Gromet (2004) and Rapela et al. (2007, 2011) proposed that the Río de la Plata craton was displaced along dextral shear zones during or after the Pampean orogeny. In this scenario, the craton did not represent the western Gondwana margin in the Córdoba area before Pampean deformation. Verdecchia et al. (2011) recently inferred that the Río de la Plata craton reached its present relative position dur-

ing the mid- to Late Cambrian, after the main Pampean tectonothermal event, whereas Iannizzotto et al. (2013) proposed a strike-slip transfer of the craton during dextral mylonitization in the Early Cambrian.

A central factor in these tectonic models is the inferred role of a thick clastic and mostly turbiditic sequence in northwest Argentina known as the Puncoviscana Formation (sensu lato). Deposition of the sequence comprises the late Neoproterozoic–Early Cambrian interval (e.g., Aceñolaza and Miller, 1982; Aceñolaza, 2003; Aceñolaza and Aceñolaza, 2005; Adams et al., 2008, 2011; Escayola et al., 2011; Toselli et al., 2012) before the Early Cambrian Pampean orogeny and subsequent unconformable clastic deposition of the Mesón Group in the early Late Cambrian (Adams et al., 2011, with discussion therein). The Puncoviscana Formation succession grades into higher-grade metamorphic rocks to the south (e.g., Willner et al., 1985; Willner and Miller, 1986; Aceñolaza et al., 1988; Willner, 1990). Metaclastic sequences in the southern and southeastern parts of the Eastern Sierras Pampeanas (e.g., Sierras de San Luis, Sierras de Córdoba; Fig. 1) have been interpreted as time equivalents of this formation (e.g., Prozzi and Ramos, 1988; Prozzi, 1990; Baldo et al., 1996; Rapela et al., 1998a, 2007; von Gosen and Prozzi, 1998; Söllner et al., 2000; von Gosen et al., 2002; Schwartz and Gromet, 2004).

Deposition of the Puncoviscana Formation sediments in a large approximately N–S–trending basin was related either to the passive margin of western Gondwana (e.g., Willner et al., 1987; Aceñolaza et al., 1988; Rapela et al., 1998a; Piñán-Llamas and Simpson, 2006; Adams et al., 2008, 2011) or a foreland basin in front of the developing Pampean orogen in the east (e.g., Kraemer et al., 1995; Keppie and Bahlburg, 1999; Zimmermann, 2005). Escayola et al. (2011) proposed that Puncoviscana Formation sediments older than 530 Ma were deposited in the arc-trench gap of the west-facing Pampean arc and/or the associated trench, whereas sediments younger than 530 Ma were deposited in a syncollision foreland basin. In the model of Rapela et al. (2007), the Neoproterozoic sediments represent a forearc sequence along the proto-Pacific Gondwana margin, affected by dextral strike-slip displacement at its eastern border, whereas deposition of the Puncoviscana Formation in an aulacogenic basin was proposed by Toselli et al. (2012).

In the northeastern continuation of the Sierras de Córdoba, the Sierra Norte de Córdoba is underlain by widely distributed granitoid intrusions (Fig. 1) commonly referred to as the Sierra Norte–Ambargasta batholith. The intrusions are thought to represent a calc-alkaline arc (e.g., Lira et al., 1997) emplaced from ca. 555 to 525 Ma,

with later peraluminous magmatism between ca. 525 and 515 Ma (Miró et al., 2005; Schwartz et al., 2008). The magmatism was related to east-directed subduction beneath the western Gondwana margin, perhaps the Río de la Plata craton (cf. Schwartz et al., 2008; von Gosen and Prozzi, 2010), and possibly combined with the approach of the Pampean terrane in the west (e.g., von Gosen and Prozzi, 2010). Subduction is interpreted as dextral oblique (von Gosen and Prozzi, 2010), leading to final oblique collision (e.g., Rapela et al., 2007; Casquet et al., 2012) with dextral transpressive kinematics (e.g., von Gosen and Prozzi, 2010; Iannizzotto et al., 2013).

The Cambrian magmatic rocks are intruded by Ordovician granitoids in the Sierra Norte and Sierras de Córdoba (e.g., Baldo et al., 1998; Rapela et al., 1998a; Bonalumi and Baldo, 2002), which are related to the Famatinian magmatic arc in the western part of the Eastern Sierras Pampeanas complex (Fig. 1). The Famatinian continental arc (Pankhurst et al., 1998, 2000; Dahlquist et al., 2008, 2013; Ducea et al., 2010) is interpreted as the product of the Upper Cambrian–Middle Ordovician subduction beneath the Eastern Sierras Pampeanas, and it was demonstrably affected by compressive deformation and metamorphism during subsequent collision of the Cuyania (Precordillera) terrane (e.g., Pankhurst et al., 1998; Rapela et al., 1998c; von Gosen and Prozzi, 1998, 2005c; von Gosen et al., 2002; Sato et al., 2003; Thomas and Astini, 2003; Astini and Dávila, 2004; González et al., 2004; Ramos, 2004; Steenken et al., 2006).

Herein, we provide U–Pb zircon data from magmatic rocks with different structural relationships to determine the timing of sedimentation and different stages of compressive deformation(s) and igneous activity in the Sierra Norte de Córdoba, representing the easternmost segment of the Eastern Sierras Pampeanas close to or at the (unexposed) Río de la Plata craton as western pre-Andean Gondwana margin. The relationships define a continuum of partitioned contractional and dextral deformation that affected clastic sedimentary sequences deposited on this margin. The new data allow regional correlation of stratigraphic and deformational histories and greatly strengthen earlier conclusions for the importance of dextral transpression during Pampean orogenesis (von Gosen and Prozzi, 2010; Iannizzotto et al., 2013).

GEOLOGIC SETTING

Intrusive rocks exposed in the Sierra Norte de Córdoba and their northern continuation in the southernmost part of the Santiago del Estero Province enclose thin N–S– to NE–SW–strick-

ing screens of low-grade metamorphic rocks (Fig. 2) that represent relics of a former widely distributed clastic sequence. The metaclastic rocks have been extensively studied (Lucero, 1958, 1969; Methol, 1958; Quartino et al., 1978; Lucero Michaut, 1979, 1981; Lucero Michaut and Daziano, 1985, 1988; Llambías et al., 2003; Martino et al., 2004; von Gosen and Prozzi,

2005b, 2009, 2010; von Gosen et al., 2009) and either assigned a Proterozoic or Proterozoic–early Paleozoic age (e.g., Lucero, 1958, 1969; Lucero Michaut, 1979, 1981) or interpreted as time equivalents of the Neoproterozoic–Early Cambrian Puncoviscana Formation of north-west Argentina (e.g., Llambías et al., 2003; von Gosen and Prozzi, 2005b, 2009, 2010; von

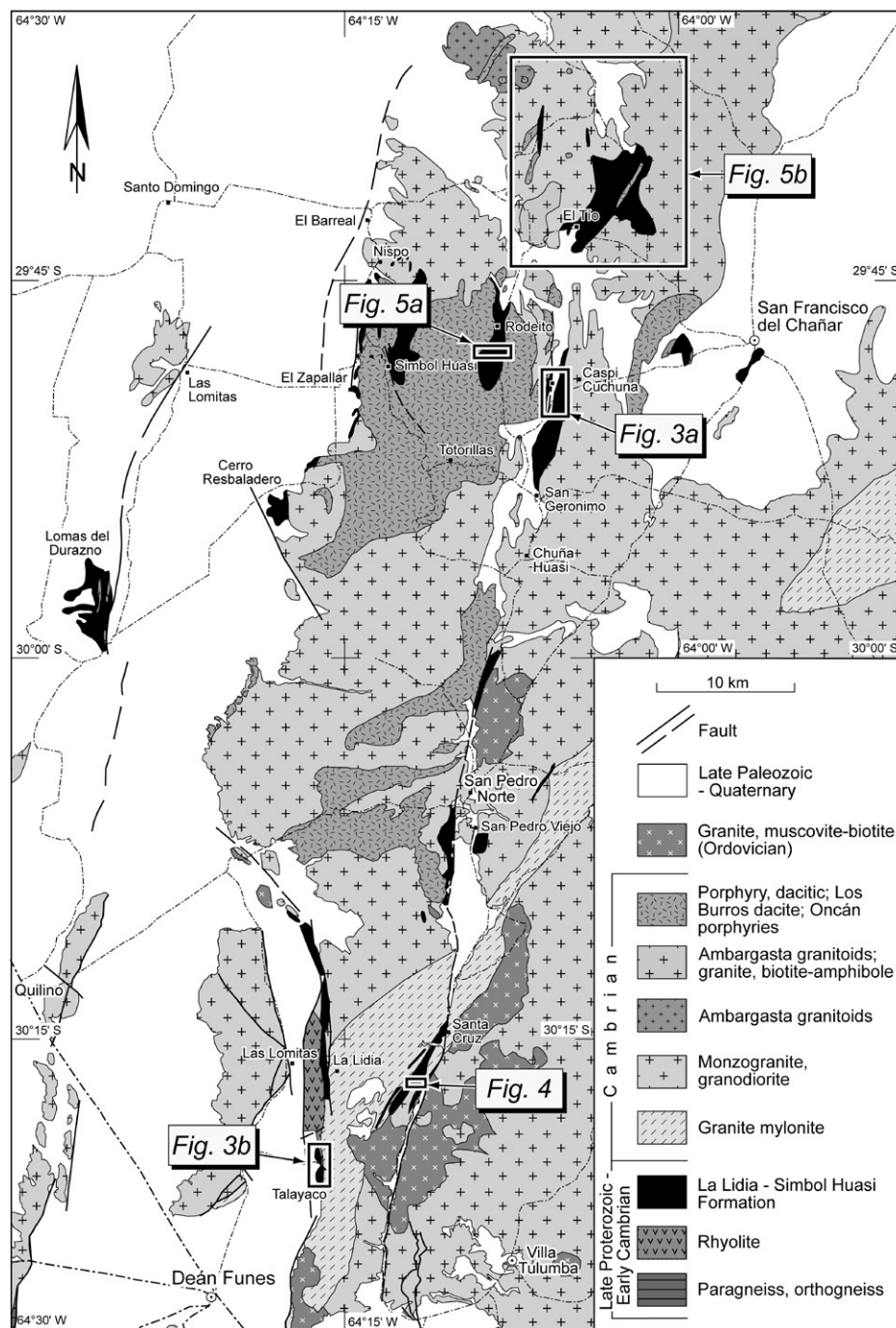


Figure 2. Geological map of the central parts of the Sierra Norte de Córdoba (modified from von Gosen and Prozzi, 2009). For location, see Figure 1. Locations of maps of Figures 3A, 3B, 4, 5A, and 5B are shown.

Gosen et al., 2009) with a southeastern extent in the Sierras de Córdoba (see previous section).

The metasedimentary rocks were assigned to the La Lidia–Simbol Huasi Formation by Lucero Michaut (1979) based on comparison with the La Lidia Formation of Beder (1922). More recent studies have shown that the sequence can be separated into two different units associated with acid meta-igneous rocks (e.g., von Gosen and Prozzi, 2005a, 2005b, 2005d, 2009, 2010). The Lower Unit, exposed in the La Lidia, Talayaco, and Agua del Río areas (Fig. 2), consists of thick metaconglomerate layers associated with metasediments, quartzite, and quartz schist interlayered with metarhyolite to metarhyodacite volcanic units. The Upper Unit includes quartzite and metasediments, with minor metasilstone to mudstone, and some intercalated metarhyolite to metadacite layers. Metaconglomerate in the Upper Unit only occurs at Rodeito and west and northwest of Simbol Huasi (Fig. 2). Minor local metaconglomerate units were also found in the El Tío and Cerro Resbaladero sections.

The clastic members of the Lower Unit have been interpreted as a fluvial to alluvial-fan section deposited in proximity to synsedimentary normal faults (von Gosen and Prozzi, 2005b, 2005d, 2009). Deposition of the Upper Unit presumably took place under continuing subsidence. The entire succession is related to a passive-margin setting, most likely on the western margin of the Río de la Plata craton (cf. von Gosen and Prozzi, 2005b, 2005d, 2009, 2010; Schwartz et al., 2008; von Gosen et al., 2009). A metarhyolitic ignimbrite at the base of the section in the La Lidia area gave a conventional thermal ionization mass spectrometry (TIMS) U-Pb zircon age of 584 ± 22 –14 Ma (Llambías et al., 2003) that was considered to be the age of crystallization by the authors. However, the ignimbrite could have included different zircon populations that might have led to a mixed age. U-Pb secondary ionization mass spectrometry (SIMS) dating of detrital zircons from a quartzite gneiss in the southernmost part of the Sierra Norte de Córdoba suggests a 560 Ma maximum age for deposition of its protolith (Iannizzotto et al., 2013). Both dates point to a maximum Neoproterozoic depositional age for the clastic units.

The clastic succession was affected by at least one compressive deformation event (D_1) that led to folding and cleavage or foliation formation. D_1 deformation is interpreted to record strain partitioning with a dextral component related to distinct shear zones (von Gosen and Prozzi, 2010). The clastic units and magmatic rocks that intrude them were locally deformed during subsequent dextral shearing and mylonitization (D_2 event: von Gosen and Prozzi, 2010; see also Miró et al., 1999; Martino,

2003; Iannizzotto et al., 2011, 2013). Metamorphism accompanying deformation ranged from subgreenschist- to lower-greenschist-facies conditions. The metasedimentary rocks have also been locally overprinted by contact metamorphism of variable grade and areal extent related to intrusive events (e.g., Guerreschi and Martino, 2002; Martino and Guerreschi, 2005).

Many published ages from this area and the adjacent southernmost part of the Santiago del Estero Province in the north are based on K-Ar and some Rb-Sr data that span the Neoproterozoic–Silurian interval (e.g., Castellote, 1982, 1985a, 1985b; Rapela et al., 1991; Koukharsky et al., 1999; Massabie et al., 2002; Millone et al., 2003; overview in Leal et al., 2003). Several U-Pb zircon ages from the Sierra Norte de Córdoba, however, give more precise time constraints (e.g., Rapela et al., 1998a, 1998b; Stuart-Smith et al., 1999; Leal et al., 2003; Llambías et al., 2003; Miró et al., 2005; Schwartz et al., 2008; Siegesmund et al., 2010; Iannizzotto et al., 2011, 2013) and point to a short-lived deformational and magmatic history. Iannizzotto et al. (2013) established an Early Cambrian age for dextral mylonitization in the southernmost part of the Sierra Norte through U-Pb zircon (SIMS) dating of the pre-/synmylonitic Juan García granodiorite (537 ± 4 Ma) and post-mylonitic Villa Albertina granite (530 ± 4 Ma).

We present U-Pb zircon data from eight magmatic rocks collected in the Sierra Norte de Córdoba, north of the Iannizzotto et al. (2013) study area, in the context of their differing structural relationships with adjacent units. In the text, we use the terms “Pampean” (latest Neoproterozoic–mid-Cambrian) and “Famatinian” (early-mid-Ordovician) for the two main orogenic events (Dahlquist et al., 2008, with references therein). Concerning the assignments of the isotopic dates, we have used the time scale of Walker et al. (2012).

SAMPLE LOCATIONS

Samples for this study were collected at localities identified during structural studies of clastic metasedimentary rocks and their contacts with extrusive and intrusive igneous rocks in the Sierra Norte area and its continuation in the southernmost part of the Santiago del Estero Province (Fig. 2; von Gosen and Prozzi, 2009, 2010). The Lower Unit, exposed in the western strip of the Agua del Río occurrence (Fig. 3A), includes vertical to overturned metaclastic rocks intercalated with several layers of foliated metarhyolite to metarhyodacite. The volcanic layers are interpreted as flows and pyroclastic deposits rather than sills. A sample of massive red metarhyolite with well-developed quartz phe-

nocrysts was taken from the northern portion of the occurrence (CE-54D; Fig. 3A).

In the south, the Talayaco metaconglomerate of the Lower Unit is intruded by a granite that is widely exposed in the east (Fig. 3B). Both the granite and the clastic succession to the west experienced compressive deformation. The metaconglomerate and enclosing quartz schist are foliated and show an increase in deformation toward the granite contact to the east. The granite at the contact is mylonitized and thrust westward over the metaconglomerate, with a local thin layer of mylonitized quartz schist within the thrust zone. West-directed reverse faulting was followed by dextral shearing, recorded by granite mylonite also east of the thrust contact (von Gosen and Prozzi, 2010). A sample was collected from the dextral mylonitic granite for U-Pb analysis (CE-56D; Fig. 3B).

The wide, NE-SW-trending strip of dextral granite mylonites south of San Pedro Norte (Fig. 2) is part of a long mylonite zone, which was named “faja de deformación Sauce Punco” by Martino et al. (1999a, 1999b) and described by Martino et al. (1999a, 1999b), Miró et al. (1999), Martino (2003), and von Gosen and Prozzi (2010). The deformation zone also contains thin bands of mylonitized schist that are interpreted as parts of the La Lidia–Simbol Huasi Formation (von Gosen and Prozzi, 2009). South of San Pedro Norte (southwest of Santa Cruz), the granite and schist mylonites are intruded by a granite porphyry (Fig. 4; von Gosen and Prozzi, 2010). At its western margin, the granite porphyry is affected by several subvertical, meter-thick mylonite zones. Northeastern exposures of the intrusion are either undeformed or locally affected by a conjugate set of thin dextral and sinistral shear zones. The shear zones die out over a short distance along strike into magmatic fabrics. The eastern margin of the intrusion contains no evidence of ductile deformation. These observations suggest that the granite porphyry intruded the mylonite zone during dextral shearing and was affected only by the final stage of the overall dextral mylonitization (von Gosen and Prozzi, 2010). Prekinematic emplacement for the intrusion is ruled out because it is not penetratively foliated and is discordant to the mylonite foliation in the country rocks at its northern margin. A sample of the synkinematic intrusion was collected east of the mylonite zone that marks the western contact of the intrusion against the mylonitized schist (CR-49D; Fig. 4).

Subvertical to slightly overturned metaclastic rocks of the Lower Unit intercalated with acid meta-igneous layers in the Agua del Río area are intruded by a coarse-grained, amphibole-bearing dacite porphyry (Fig. 3A). The country rocks

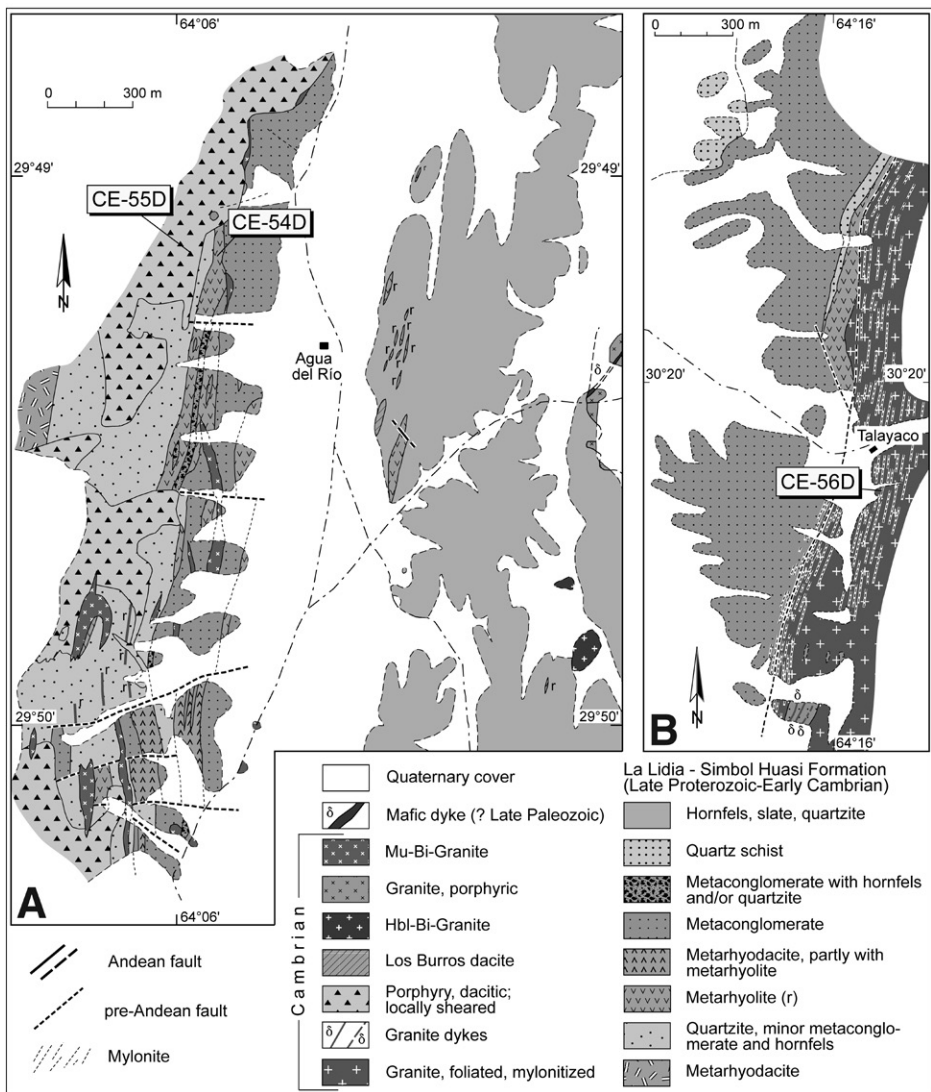


Figure 3. Geological maps of the central part of the (A) Agua del Río and (B) Talayaco occurrences of clastic metasedimentary rocks and acid magmatic rocks (modified from von Gosen and Prozzi, 2009). For location of maps, see Figure 2. Bi—biotite, Hbl—hornblende, Mu—muscovite. Locations of samples for isotopic dating are shown.

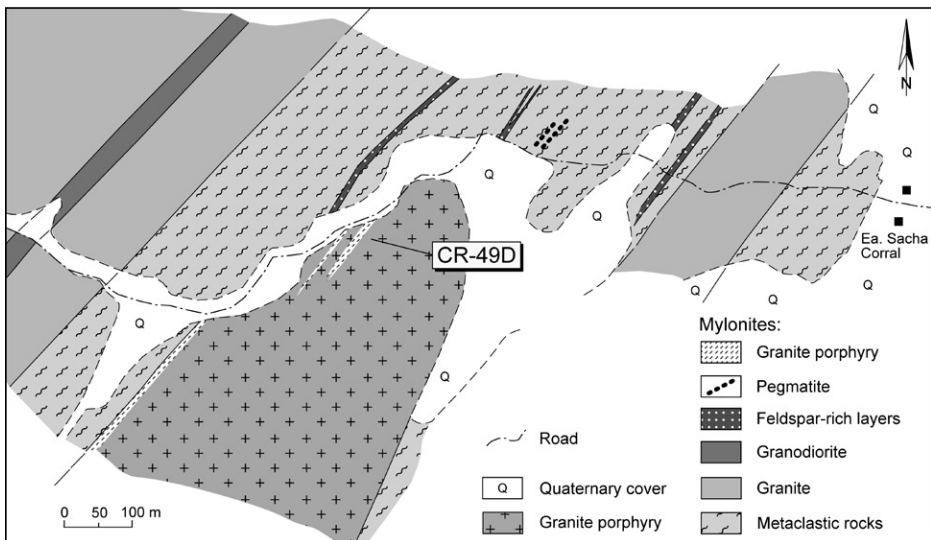


Figure 4. Simplified sketch map of mylonites and intrusions in the area south of San Pedro Norte, west of Estancia Sacha Corral, modified from von Gosen and Prozzi (2010). Location of map is indicated in Figure 2. Location of sample CR-49D in the granite porphyry is shown.

were foliated and rotated into the subvertical position before emplacement of the intrusion, and the porphyry is locally dextrally sheared at its eastern intrusive margin (von Gosen and Prozzi, 2010). Thus, the emplacement probably took place during the final stage of Pampean compressive deformation. Minor deformation at its eastern contact indicates that intrusion of the porphyry was late synkinematic with shearing active during cooling. A sample of the dacite porphyry was taken in the northern part of the

Agua del Río occurrence (CE-55D; Fig. 3A), west of the sheared intrusive margin where the rock was affected by only a weak deformation.

Deformed metaclastic rocks and intercalated acid meta-igneous rocks in the eastern portion of the large exposure in the El Tío area (Fig. 5B) are intruded by a porphyritic biotite-amphibole granite (El Tío granite) that is included with the Cambrian Ambargasta granitoids (e.g., Miró and Sapp, 2000). The granite contains angular xenoliths of the foliated clastic country rocks with dif-

ferent sizes. Chilled margins occur at the xenolith contacts, suggesting a high level of granite intrusion with brittle fracturing of the crust (von Gosen and Prozzi, 2010). The intrusion produced contact metamorphism of the deformed country rocks. The granite was not ductilely deformed. A sample was collected from the intrusion near its southern contact with the metaclastic country rocks (CE-66D; Fig. 5B).

Folded and cleaved rocks of the approximately NNE-SSW-striking metaclastic succession in the Rodeito area (Fig. 2) are intruded by a hypabyssal rhyolite to dacite. The intrusion also cuts the thin layer of the Rodeito metaconglomerate. A sample of the intrusion was collected just west of the metaconglomerate (CD-22D; Fig. 5A).

The small El Escondido occurrence of clastic rocks in the southernmost Santiago del Estero Province (Fig. 1) lies in a morphological depression between the Sierra de Ambargasta to the west and Sierra de Sumampa to the east (Fig. 6). The El Escondido Formation sandstones and conglomerates record synsedimentary folding but are not ductilely deformed (Martino, 2004; von Gosen et al., 2005). They are entirely different from the low-grade clastic rocks in the Sierra Norte de Córdoba, hornfeldes in the La Clemira area, and medium-grade metamorphic rocks of the Pozo del Macho Formation (Castellote, 1985b) and equivalents in the east and southeast. The clastic rocks depositionally overlie a basal rhyolite in the El Escondido area. The rhyolite is intruded by a granite that does not cut but appears as angular clasts in the overlying sedimentary rocks of the El Escondido Formation (Fig. 5C; Martino, 2004; von Gosen et al., 2005). A sample was taken from the undeformed rhyolite beneath the El Escondido Formation sedimentary rocks (CD-7D). A sample of the El Escondido granite was analyzed to obtain a maximum age for the El Escondido clastic deposits and a minimum age for the Pampean igneous history (CD-8D; Fig. 5C).

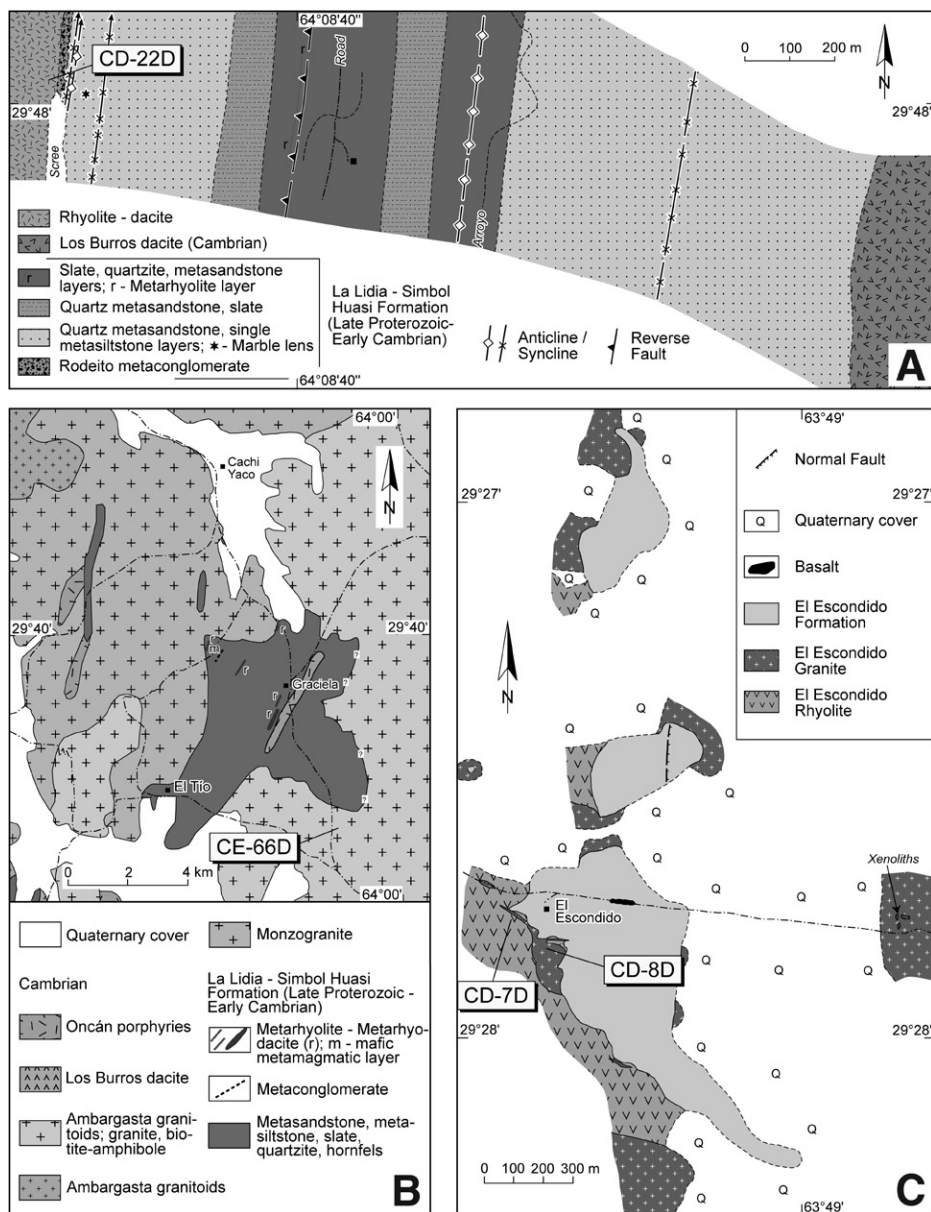


Figure 5. (A) Sketch map of the lithology in the central part of the Rodeito occurrence of clastic metasedimentary and acid magmatic rocks. Map is based on our field work. (B) Geological map of the El Tío area, modified from von Gosen and Prozzi (2010). (C) Geological sketch map of the El Escondido occurrence west of Villa Ojo de Agua (Santiago del Estero), based on our own field work. In the maps, the sample locations are shown. For locations of maps A and B, see Figure 2; location of map C is shown in Figure 6.

DESCRIPTIONS AND AGES OF THE ZIRCONS

Zircons for this study were analyzed as fractions of one to three grains using the thermal ionization mass spectrometry (TIMS) method and/or by the secondary ionization mass spectrometry (SIMS) method. SIMS analyses were employed on samples analyzed by the TIMS method to help resolve problems associated with inheritance and Pb loss. The sample preparation and analytical procedures for each method are summarized in Appendixes 1–3. The results of the SIMS analyses are shown in Table 1. The results of the TIMS analyses are presented in

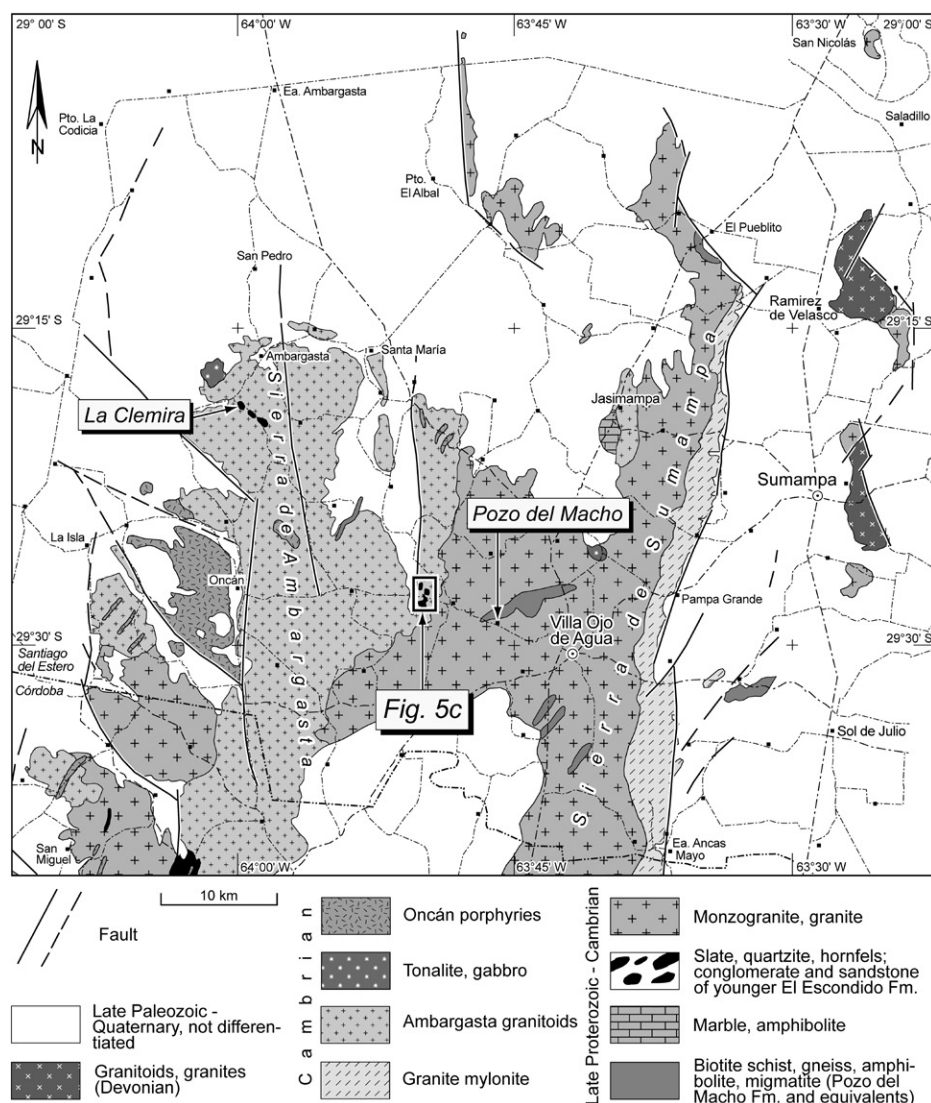


Figure 6. Geological map of the Sierras de Ambargasta and Sumampa in the southernmost part of the Santiago del Estero Province (after Miró and Sapp, 2000; location of map is shown in Fig. 1). The locations of the El Escondido occurrence (map of Fig. 5C), La Clemira, and Pozo del Macho are shown.

Table DR1 and Figures DR1–DR3.¹ Although the TIMS results are not extensively discussed in the text, the data are presented because they provide insight into the complex zircons observed in these samples, demonstrate some of the undetected problems with other published data, and provide a rationale for integrated SIMS and chemical-abrasion TIMS (Mattinson, 2005) analysis in future work. Rare earth element (REE) data collected simultaneously with

¹GSA Data Repository Item 2014169, Table DR1 and Figures DR1 to DR3, thermal ionization mass spectrometry data, is available at www.geosociety.org/pubs/ft2014.htm, or on request from editing@geosociety.org, Documents Secretary, GSA, P.O. Box 9140, Boulder, CO 80301-9140, USA.

the SIMS U-Pb analyses help to distinguish disturbed and undisturbed zircon populations and are presented in Table 2. The age results provide time markers for the sedimentary, tectonic, and igneous histories in this easternmost part of the Eastern Sierras Pampeanas unit.

The zircon crystals analyzed from the meta-ryholite of the Agua del Río occurrence (CE-54D) are middle to long prismatic, colorless clear, or have a slight honey-like color. Grains show clear oscillatory growth zoning with some inherited cores, opaque inclusions, and zones of resorption/recrystallization (Fig. 7A). SIMS analysis of oscillatory zoned domains gave ²⁰⁷Pb-corrected ²⁰⁶Pb/²³⁸U ages ranging from 495 to 546 Ma. Assuming the younger ages reflect Pb loss, as is demonstrated by the TIMS data for

this sample (Fig. DR1 [see footnote 1]), 7 of 12 zircon analyses give a concordia age of 535 ± 5 Ma (Fig. 7B), which is interpreted as the crystallization age of the metarhyolite. The light REE elements (LREEs) are variable for three of the analyses (Fig. 8A), but there is little correlation of REE disturbance with observed U-Pb age.

The analyzed zircons from the granite mylonite at Talayaco (CE-56D) are short prismatic, partly isometric, and colorless to pale white. In cathodoluminescence (CL) images, the grains are oscillatory zoned with occasional cores (Fig. 9A). The SIMS results gave ²⁰⁷Pb-corrected ²⁰⁶Pb/²³⁸U ages ranging from 478 to 547 Ma. The LREEs in roughly half of the grains are elevated (Fig. 8B), indicating modification of the original igneous signature by alteration. The disturbed REE patterns are associated with younger ²⁰⁶Pb/²³⁸U ages. Assuming discordance is due to Pb loss, the oldest nine analyses give a concordia age of 533 ± 4 Ma (Fig. 9B).

The granite porphyry sample CR-49D has colorless short prismatic to elongate zircons with oscillatory zoned mantles that surround either similarly zoned cores or obvious cores with irregular zoning patterns (Fig. 10A) that might be related to rapid growth in the melt. Thin (5–20 μm) CL-dark, higher-U rims are present on roughly half of the grains. Single-grain TIMS analyses demonstrate significant Pb loss (Fig. DR2 [see footnote 1]), whereas the SIMS data show complexities of combined inheritance and Pb loss (Fig. 10B). SIMS analyses from domains that have suffered Pb loss are generally associated with elevated LREE patterns (Fig. 8C). Excluding older inherited cores and younger ages associated with disturbed REE concentrations, 6 of 16 analyses provide a weighted mean ²⁰⁶Pb/²³⁸U age of 534 ± 5 Ma (Fig. 10B). We interpret this date as the age of zircon crystallization.

Zircons from the Agua del Río dacitic porphyry (CE-55D) yielded stubby to elongate, prismatic, colorless zircons with opaque and colorless inclusions common and no obvious cores (Fig. 11A). The grains have well-developed oscillatory zoning, with thick (10–30 μm) CL-dark, higher-U rims common. SIMS analyses targeting uniform oscillatory zoned domains, including the higher-U rims, have uniform REE patterns (Fig. 8D), and 15 of 16 U-Pb analyses give a concordia age of 531 ± 4 Ma (Fig. 11B). One younger SIMS analysis and the scatter observed in the TIMS data (Fig. DR3 [see footnote 1]) are attributed to Pb loss.

The colorless clear zircons from the El Tío granite (CE-66D) are subequant to elongate, euhedral, and oscillatory zoned grains (Fig. 12A). Most grains have CL-dark, higher-U rims, and a minor subset of the population shows

TABLE 1. SECONDARY IONIZATION MASS SPECTROMETRY (SIMS) U-Pb GEOCHRONOLOGIC DATA AND APPARENT AGES

Spot [†]	CL [†]	U (ppm)	Th (ppm)	Th/U	²⁰⁶ Pb* _s (ppm)	²⁰⁸ Pb _c §	²³⁸ U/ ²⁰⁶ Pb [#]	²⁰⁷ Pb/ ²⁰⁶ Pb [#]	²⁰⁶ Pb/ ²³⁸ U** (Ma)	²⁰⁷ Pb/ ²⁰⁶ Pb (Ma)		
Sample CE-54D												
1.1	om	490	232	0.49	36	0.13	11.624	(1.1)	.05908	(1.0)	531	(6)
2.1	om	414	187	0.47	31	0.03	11.663	(1.1)	.05822	(1.2)	530	(6)
3.1	om	297	142	0.49	22	0.01	11.620	(1.0)	.05814	(1.4)	532	(5)
4.1	om	495	273	0.57	38	0.02	11.312	(0.9)	.05860	(1.0)	546	(5)
5.1	om	398	209	0.54	29	0.09	11.907	(1.0)	.05847	(1.2)	519	(5)
6.1	om	114	44	0.40	9	<0.01	11.421	(1.1)	.05755	(2.1)	542	(6)
7.1	c	176	130	0.77	13	0.45	11.306	(1.1)	.06204	(1.7)	544	(6)
8.1	c	111	72	0.68	8	0.35	12.499	(1.2)	.05992	(2.2)	495	(6)
9.1	om	309	163	0.55	22	<0.01	12.161	(1.0)	.05640	(1.4)	510	(5)
10.1	om	240	113	0.49	18	<0.01	11.616	(1.0)	.05670	(1.5)	533	(5)
11.1	c	171	82	0.50	13	<0.01	11.607	(1.1)	.05685	(1.7)	534	(6)
12.1	om	243	127	0.54	17	0.14	12.075	(1.0)	.05869	(1.5)	512	(5)
Sample CE-56D												
1.1	r	410	142	0.36	29	0.30	12.008	(0.9)	.06007	(1.1)	514	(5)
2.1	c	432	123	0.29	32	0.08	11.637	(0.9)	.05866	(1.6)	531	(5)
3.1	om	304	158	0.54	23	0.15	11.597	(0.9)	.05929	(1.3)	532	(5)
4.1	c	811	309	0.39	60	0.06	11.687	(0.8)	.05843	(0.8)	529	(4)
5.1	c	779	404	0.54	56	0.36	11.905	(0.9)	.06060	(0.9)	518	(4)
6.1	c	202	151	0.77	13	0.36	12.954	(1.0)	.05955	(1.7)	478	(5)
7.1	c	204	77	0.39	14	0.30	12.169	(1.0)	.05987	(1.7)	508	(5)
8.1	om	777	591	0.79	56	0.06	11.888	(0.9)	.05826	(0.9)	520	(4)
9.1	om	1063	410	0.40	77	0.07	11.787	(0.8)	.05847	(0.7)	525	(4)
10.1	c	1049	338	0.33	76	0.20	11.887	(0.8)	.05936	(0.7)	520	(4)
11.1	om	304	141	0.48	22	0.14	11.913	(0.9)	.05888	(1.2)	519	(5)
12.1	c	285	168	0.61	21	<0.01	11.422	(0.9)	.05772	(1.2)	541	(5)
13.1	c	557	283	0.52	41	0.05	11.707	(0.9)	.05835	(1.1)	528	(4)
14.1	c	197	95	0.50	15	<0.01	11.310	(1.0)	.05790	(1.5)	547	(5)
15.1	om	1003	415	0.43	74	0.07	11.652	(0.8)	.05855	(0.7)	530	(4)
16.1	c	576	184	0.33	42	0.06	11.738	(0.9)	.05841	(0.9)	527	(5)
Sample CR-49D												
1.1	c	134	57	0.44	10	0.03	11.441	(1.1)	.05853	(1.8)	540	(6)
2.1	c	260	67	0.27	15	1.56	15.157	(1.0)	.06747	(1.9)	406	(4)
3.1	om	195	76	0.40	14	<0.01	11.742	(1.0)	.05743	(1.5)	527	(5)
4.1	om	214	111	0.54	16	0.09	11.351	(1.0)	.05910	(1.4)	544	(5)
5.1	om	142	54	0.39	11	0.13	11.468	(1.1)	.05931	(1.7)	538	(6)
6.1	c	333	86	0.27	60	0.04	4.805	(0.9)	.08121	(0.7)	1218	(11)
7.1	om	185	94	0.52	14	0.08	11.739	(1.0)	.05857	(1.5)	527	(5)
8.1	om	312	253	0.84	17	1.50	15.459	(0.9)	.06674	(1.2)	398	(4)
9.1	om	194	67	0.36	12	1.84	13.350	(1.0)	.07108	(1.4)	457	(5)
10.1	om	194	119	0.64	14	0.08	11.624	(1.0)	.05872	(1.5)	532	(5)
11.1	r	521	81	0.16	36	1.52	12.267	(0.9)	.06952	(1.1)	498	(4)
12.1	r	1028	342	0.34	40	4.70	21.934	(0.8)	.08941	(0.9)	274	(2)
13.1	r	247	252	1.05	18	0.27	11.823	(1.0)	.06000	(1.3)	522	(5)
14.1	c	200	184	0.95	16	1.00	10.569	(1.0)	.06746	(1.5)	577	(6)
15.1	c	21	14	0.67	3	10.09	6.166	(4.9)	.15208	(7.5)	877	(44)
16.1	c	3023	593	0.20	84	16.27	30.751	(0.9)	.17931	(6.1)	173	(3)
Sample CE-55D												
1.1	om	148	102	0.71	11	0.05	11.70	(1.1)	.05835	(1.9)	529	(6)
2.1	om	229	157	0.71	17	<0.01	11.64	(1.0)	.05751	(1.6)	532	(5)
3.1	om	129	82	0.66	9	0.43	12.37	(1.1)	.06066	(2.0)	499	(5)
4.1	c	164	156	0.99	12	0.15	11.75	(1.1)	.05909	(1.8)	526	(5)
5.1	om	214	108	0.52	16	<0.01	11.51	(1.0)	.05729	(1.6)	538	(5)
6.1	om	174	100	0.59	13	0.06	11.73	(1.0)	.05844	(1.8)	527	(5)
7.1	c	168	133	0.82	12	0.12	11.94	(1.1)	.05866	(1.8)	518	(5)
8.1	c	91	78	0.89	7	<0.01	11.45	(1.2)	.05781	(2.5)	540	(7)
9.1	om	165	105	0.66	12	0.14	11.71	(1.1)	.05907	(1.8)	527	(5)
10.1	c	132	66	0.51	10	<0.01	11.82	(1.2)	.05570	(2.6)	525	(6)
10.2	r	297	138	0.48	22	<0.01	11.77	(1.0)	.05611	(2.1)	527	(5)
11.1	c	273	188	0.71	20	0.04	11.49	(1.0)	.05854	(1.3)	538	(5)
12.1	om	143	108	0.78	11	<0.01	11.63	(1.1)	.05747	(2.5)	532	(6)
13.1	om	257	107	0.43	19	<0.01	11.57	(1.0)	.05805	(1.4)	535	(5)
14.1	c	101	72	0.74	7	<0.01	11.70	(1.2)	.05644	(2.2)	530	(6)
15.1	c	285	195	0.71	21	0.01	11.72	(1.0)	.05807	(1.2)	528	(5)
Sample CE-66D												
1.1	om	278	94	0.35	20	<0.01	11.703	(1.0)	.05785	(1.5)	529	(5)
2.1	om	559	257	0.47	41	<0.01	11.587	(1.0)	.05793	(1.1)	534	(5)
3.1	r	232	91	0.41	18	<0.01	11.340	(1.1)	.05841	(1.6)	545	(6)
4.1	om	126	55	0.45	9	0.20	11.785	(1.2)	.05951	(2.1)	524	(6)

(continued)

TABLE 1. SECONDARY IONIZATION MASS SPECTROMETRY (SIMS) U-Pb GEOCHRONOLOGIC DATA AND APPARENT AGES (continued)

Spot [†]	CL [†]	U (ppm)	Th (ppm)	Th/U	²⁰⁶ Pb* _s (ppm)	²⁰⁶ Pb _c [‡]	²³⁸ U/ ²⁰⁶ Pb [#]	²⁰⁷ Pb/ ²⁰⁶ Pb [#]	²⁰⁶ Pb/ ²³⁸ U** (Ma)	²⁰⁷ Pb/ ²⁰⁶ Pb (Ma)		
Sample CE-66D												
5.1	om	188	65	0.36	14	<0.01	11.498	(1.0)	.05811	(1.7)	538	(6)
6.1	om	284	124	0.45	22	<0.01	11.076	(1.0)	.05825	(1.3)	558	(5)
7.1	om	318	140	0.45	24	<0.01	11.295	(1.0)	.05753	(1.3)	547	(5)
8.1	om	751	242	0.33	56	0.25	11.599	(0.9)	.06013	(0.8)	532	(5)
9.1	om	337	118	0.36	25	<0.01	11.803	(1.0)	.05696	(1.2)	525	(5)
10.1	om	712	100	0.15	11	10.07	53.485	(1.0)	.12818	(1.0)	107	(1)
11.1	c	286	175	0.63	21	<0.01	11.577	(1.0)	.05674	(1.3)	535	(5)
12.1	om	157	59	0.39	12	0.05	10.978	(1.1)	.05923	(1.7)	562	(6)
Sample CD-22D												
1.1	c	182	139	0.79	13	0.01	11.640	(1.0)	.05812	(1.5)	531	(5)
2.1	om	166	93	0.58	12	<0.01	11.670	(1.0)	.05757	(1.8)	530	(5)
3.1	c	118	61	0.54	9	0.13	11.897	(1.1)	.05880	(2.1)	520	(6)
4.1	om	218	104	0.49	16	0.20	11.598	(1.0)	.05970	(1.6)	532	(5)
5.1	c	120	98	0.85	9	0.22	11.863	(1.2)	.05955	(2.2)	521	(6)
6.1	c	86	53	0.64	6	<0.01	11.708	(1.2)	.05732	(2.5)	529	(6)
7.1	r	293	162	0.57	21	0.32	12.076	(0.9)	.06013	(1.3)	511	(5)
7.2	c	162	104	0.66	12	0.34	12.044	(1.1)	.06033	(1.8)	512	(6)
8.1	om	252	153	0.63	19	0.31	11.556	(1.0)	.06064	(1.5)	533	(5)
9.1	c	460	295	0.66	33	1.33	11.944	(0.9)	.06834	(1.0)	512	(4)
9.2	r	752	764	1.05	43	6.04	14.882	(0.8)	.10339	(0.9)	395	(3)
10.1	c	165	148	0.93	12	0.05	11.704	(1.1)	.05835	(1.9)	528	(5)
11.1	c	156	87	0.58	12	0.34	11.445	(1.1)	.06099	(1.8)	538	(6)
12.1	c	209	130	0.64	16	0.22	11.177	(1.0)	.06034	(1.7)	551	(6)
13.1	c	90	74	0.85	7	<0.01	11.743	(1.4)	.05727	(2.4)	527	(7)
14.1	om	423	221	0.54	32	0.28	11.390	(1.0)	.06060	(1.1)	541	(5)
15.1	c	222	128	0.60	14	1.47	13.927	(1.0)	.06760	(1.4)	441	(4)
16.1	c	167	91	0.56	13	<0.01	11.431	(1.1)	.05797	(1.7)	541	(6)
Sample CD-7D												
1.1	om	408	455	1.15	29	0.07	11.892	(0.9)	.05833	(1.2)	520	(5)
2.1	om	385	93	0.25	28	0.22	11.891	(0.9)	.05952	(1.2)	519	(5)
2.2	c	550	218	0.41	38	0.43	12.289	(0.9)	.06079	(1.0)	502	(4)
3.1	r	3869	514	0.14	68	17.02	48.827	(0.8)	.18338	(0.5)	109	(1)
3.2	c	172	100	0.60	13	0.04	11.786	(1.1)	.05817	(1.9)	525	(5)
4.1	r	1491	189	0.13	65	3.40	19.786	(0.8)	.07985	(1.2)	307	(3)
5.1	om	350	155	0.46	25	0.25	12.123	(1.2)	.05950	(1.3)	510	(6)
6.1	r	1966	806	0.42	80	8.60	21.176	(0.8)	.12065	(0.9)	272	(2)
6.2	c	83	112	1.40	6	0.34	11.898	(1.3)	.06047	(4.8)	519	(7)
7.1	om	674	185	0.28	36	2.33	15.963	(0.9)	.07307	(0.9)	383	(3)
8.1	om	158	128	0.84	12	<0.01	11.754	(1.1)	.05681	(2.9)	527	(6)
9.1	c	204	189	0.96	14	0.55	12.473	(1.0)	.06153	(1.6)	495	(5)
10.1	r	886	125	0.15	38	5.75	20.267	(0.9)	.09835	(1.0)	293	(3)
10.2	om	511	108	0.22	36	0.84	12.301	(0.9)	.06403	(1.1)	500	(4)
11.1	om	475	325	0.71	34	0.06	12.135	(0.9)	.05799	(1.1)	510	(4)
Sample CD-8D												
1.1	c	93	158	1.75	7	0.04	11.756	(1.4)	.05821	(2.3)	526	(7)
2.1	c	92	120	1.35	7	<0.01	11.375	(1.2)	.05790	(2.2)	543	(7)
3.1	om	550	300	0.56	41	0.23	11.526	(0.9)	.06002	(0.9)	535	(5)
4.1	c	179	49	0.28	13	<0.01	11.508	(1.0)	.05750	(1.6)	538	(5)
5.1	om	189	97	0.53	14	<0.01	11.417	(1.0)	.05822	(1.5)	541	(5)
6.1	c	103	117	1.18	7	0.37	13.168	(1.2)	.05948	(2.0)	470	(6)
7.1	c	320	358	1.15	23	0.11	11.748	(0.9)	.05876	(1.2)	526	(5)
8.1	c	90	122	1.39	6	0.23	11.971	(1.2)	.05954	(3.0)	516	(6)
9.1	om	205	178	0.90	15	0.04	11.825	(1.0)	.05815	(1.5)	523	(5)
10.1	c	169	249	1.52	12	0.14	11.846	(1.1)	.05889	(1.7)	522	(5)
11.1	c	74	56	0.78	5	<0.01	12.965	(1.2)	.05629	(2.6)	479	(6)
12.1	c	56	59	1.09	4	0.15	12.010	(1.4)	.05881	(2.8)	515	(7)
13.1	c	86	152	1.82	6	0.17	11.972	(1.3)	.05906	(2.3)	516	(6)
14.1	c	156	187	1.24	11	<0.01	11.852	(1.1)	.05644	(1.7)	523	(5)
15.1	c	172	257	1.55	12	0.09	11.882	(1.0)	.05852	(1.6)	520	(5)
16.1	om	107	104	1.01	8	0.52	12.015	(1.1)	.06176	(1.9)	513	(6)

Note: All analyses were performed on the sensitive high-resolution ion microprobe–reverse geometry (SHRIMP-RG) at the U.S. Geological Survey–Stanford Micro-analytical Center at Stanford University. The analytical routine followed Barth and Wooden (2006). Data reduction utilized the SQUID program of Ludwig (2005).
[†]Abbreviations: 1.1 = grain number and spot number. Cathodoluminescence (CL) designations: c—core; om—oscillatory zoned mantle; r—rim.
[‡]Pb* denotes radiogenic Pb; Pb_c denotes common Pb; ²⁰⁶Pb_c = 100 × (²⁰⁶Pb/²⁰⁶Pb_{total}).

[#]Calibration concentrations and isotopic compositions were based on replicate analyses of CZ3 (550 ppm U) and R33 (419 Ma; Black et al., 2004). Reported ratios are not corrected for common Pb. Errors are reported in parentheses as percent at the 1σ level.

**Ages were calculated from ²⁰⁶Pb/²³⁸U ratios corrected for common Pb using the ²⁰⁷Pb method (see Williams, 1998). Initial common Pb isotopic composition was approximated from Stacey and Kramers (1975). Uncertainties in millions of years are reported as 1σ. Ages in italics were omitted from age calculations discussed in the text.

TABLE 2. ZIRCON TRACE ELEMENT DATA

Spot [†]	CL [†]	Y	La	Ce	Nd	Sm	Eu	Gd	Dy	Er	Yb	Lu	Hf (×10 ³)	Ce/Ce*	Eu/Eu*	Yb _(N) /Gd _(N)
Sample CE-54D																
1.1	om	1275	21.75	57	11.8	4.5	0.46	25	102	227	470	92	13	2	0.13	23.1
2.1	om	1174	0.009	25	0.45	1.5	0.26	17	91	211	447	89	14	363	0.16	32.2
3.1	om	732	0.018	18	0.26	0.9	0.20	10	55	132	292	59	13	195	0.21	34.2
4.1	om	1128	0.736	28	0.66	1.6	0.30	16	86	201	430	85	13	19	0.18	32.1
5.1	om	1103	20.48	54	9.35	3.4	0.44	20	88	198	421	82	13	2	0.16	25.2
6.1	om	755	0.004	9	0.43	1.4	0.50	16	69	137	264	51	10	224	0.32	19.5
7.1	c	1627	0.038	21	1.51	4.0	1.03	38	147	274	481	90	11	77	0.25	15.3
8.1	c	1590	14.29	30	9.19	9.0	1.71	50	169	264	419	78	10	1	0.24	10.1
9.1	om	1130	0.004	22	0.62	1.8	0.42	20	92	200	396	77	13	462	0.21	24.3
10.1	om	1613	0.253	31	1.13	3.2	0.82	31	145	299	548	105	11	36	0.25	21.1
11.1	c	829	0.030	17	0.49	1.4	0.37	14	66	149	318	64	12	105	0.25	26.6
12.1	om	702	0.011	19	0.40	1.0	0.29	11	55	129	291	59	13	252	0.26	30.9
Sample CE-56D																
1.1	r	1325	43.3	714	36.7	20.1	4.38	55	141	248	440		11	8	0.40	9.7
2.1	c	1609	0.077	9	0.44	1.6	0.43	22	138	314	609		11	31	0.22	33.6
3.1	om	1274	0.024	19	0.69	2.4	0.42	26	123	240	439		12	124	0.16	20.5
4.1	c	3571	0.240	8	1.46	4.4	1.03	60	340	676	1158		12	9	0.19	23.3
5.1	c	3197	0.115	14	1.44	5.1	1.48	66	327	611	990		11	25	0.24	18.0
6.1	c	1722	14.8	1344	50.4	48.2	11.23	125	213	297	456		10	29	0.44	4.4
7.1	c	823	0.645	82	3.23	3.9	1.09	21	82	155	291		12	36	0.37	17.0
8.1	om	4953	6.45	108	19.7	22.5	6.26	158	560	902	1333		10	6	0.32	10.2
9.1	om	2734	0.162	16	0.95	2.9	0.77	43	245	514	951		12	27	0.21	26.9
10.1	c	3200	0.016	7	0.33	2.2	0.56	41	275	621	1112		12	79	0.18	32.6
11.1	om	1294	1.27	315	7.45	8.7	2.11	41	145	248	436		12	66	0.34	13.0
12.1	c	1446	0.026	21	1.08	3.1	0.59	32	145	270	478		13	111	0.18	18.0
13.1	c	3031	0.720	26	3.16	7.0	1.96	72	304	542	852		12	11	0.26	14.3
14.1	c	916	0.024	17	0.41	1.6	0.36	19	88	173	312		13	130	0.20	20.0
15.1	om	3719	0.738	18	2.64	4.4	1.15	54	325	688	1197		12	8	0.23	26.6
16.1	c	2226	0.047	7	0.53	2.1	0.56	31	192	436	855		11	33	0.21	33.4
Sample CR-49D																
1.1	c	1204	0.021	7	0.73	2.28	0.29	25	115	221	384		11	51	0.11	18.6
2.1	c	1230	3.12	114	11.1	14.5	0.83	52	147	212	386		12	12	0.09	9.0
3.1	om	1457	0.026	6	0.67	2.67	0.31	29	142	273	490		12	37	0.11	20.4
4.1	om	1718	0.020	10	1.27	3.66	0.44	38	174	316	544		11	60	0.11	17.1
5.1	om	1025	0.032	6	0.61	2.14	0.27	21	98	190	341		11	36	0.12	19.5
6.1	c	752	0.048	15	0.50	1.57	0.17	16	74	138	243		11	68	0.10	18.0
7.1	om	1208	0.318	27	1.23	2.78	0.22	26	116	214	364		11	26	0.08	17.2
8.1	om	1352	3.69	142	10.5	12.8	0.94	51	169	235	384		10	13	0.11	9.1
9.1	om	1567	2.19	29	6.13	8.23	0.56	44	162	277	481		11	5	0.09	13.3
10.1	om	1626	0.030	12	1.27	3.79	0.39	38	163	290	488		11	54	0.10	15.5
11.1	r	1989	8.11	240	14.8	10.0	0.84	59	176	297	539		6	12	0.10	10.9
12.1	r	3527	15.1	283	41.1	49.3	2.38	178	551	582	899		11	7	0.08	6.1
13.1	r	1850	0.300	90	1.81	3.56	1.81	36	161	341	663		10	80	0.48	22.2
14.1	c	1054	2.34	57	7.32	4.80	2.34	27	95	176	326		8	8	0.62	14.5
15.1	c	257	10.01	27	4.10	0.43	0.86	10	23	39	79		5	2	1.27	9.7
16.1	c	16723	148	1861	345	319	15.42	1131	2957	2722	4604		16	5	0.08	4.9
Sample CE-55D																
1.1	om	949	0.014	16	0.87	2.2	0.81	20	88	178	342		9	143	0.37	20.6
2.1	om	704	0.168	21	0.87	1.4	0.43	12	57	133	304		11	35	0.32	31.6
3.1	om	620	1.04	17	1.23	1.6	0.37	11	55	117	252		9	8	0.27	27.7
4.1	c	2315	0.254	19	3.81	7.6	2.80	71	253	413	634		9	14	0.37	10.8
5.1	om	1422	0.021	17	0.80	2.3	0.81	23	114	269	561		10	116	0.34	29.0
6.1	om	610	0.017	14	0.26	0.8	0.22	9	47	117	286		11	156	0.26	39.9
7.1	c	1890	0.333	24	3.33	6.3	1.97	51	195	344	559		10	17	0.33	13.2
8.1	c	1397	0.025	13	2.15	4.8	1.78	40	147	249	400		9	56	0.39	12.0
9.1	om	710	0.078	18	0.48	1.1	0.37	11	57	136	316		11	59	0.31	34.1
10.1	c	786	0.031	15	0.56	1.6	0.56	17	74	150	278		10	92	0.34	20.3
10.2	r	940	0.022	22	0.54	1.5	0.34	16	79	186	393		12	165	0.21	29.8
11.1	c	1030	0.752	26	3.75	2.8	0.63	20	87	193	414		12	10	0.26	25.3
12.1	om	778	0.023	20	0.41	1.3	0.38	15	70	146	294		12	164	0.26	24.3
13.1	om	865	0.020	16	0.25	1.1	0.26	13	75	167	361		12	169	0.21	32.9
14.1	c	1106	0.026	14	1.21	3.0	1.02	28	117	205	348		10	73	0.33	15.0
15.1	c	1534	0.021	25	1.22	3.4	0.91	33	149	295	568		12	150	0.26	21.0

(continued)

TABLE 2. ZIRCON TRACE ELEMENT DATA (continued)

Spot [†]	CL [†]	Y	La	Ce	Nd	Sm	Eu	Gd	Dy	Er	Yb	Lu	Hf ($\times 10^3$)	Ce/Ce*	Eu/Eu*	Yb _(N) /Gd _(N)
Sample CE-66D																
1.1	om	665	0.004	11	0.36	1.1	0.31	11	50	117	264	55	12	298	0.27	28.1
2.1	om	865	0.037	20	0.46	1.5	0.37	16	73	157	323	63	13	115	0.23	24.8
3.1	r	372	0.004	9	0.25	0.7	0.21	6	29	64	146	30	11	258	0.30	27.3
4.1	om	781	0.013	10	0.57	1.5	0.50	15	67	139	280	55	10	107	0.33	23.1
5.1	om	1110	0.013	14	0.76	2.0	0.62	20	88	199	406	80	10	134	0.30	24.8
6.1	om	1712	1.21	19	3.68	5.9	1.56	47	173	298	515	95	11	5	0.28	13.3
7.1	om	988	17.46	44	9.79	4.3	0.56	21	83	177	372	73	12	1	0.18	21.0
8.1	om	812	0.014	12	0.62	1.6	0.45	15	65	141	305	63	11	125	0.29	25.3
9.1	om	638	0.082	12	0.36	1.0	0.32	10	49	116	274	58	12	44	0.30	32.9
10.1	om	1372	26.02	129	34.0	23.1	2.17	69	162	230	377	67	8	2	0.17	6.6
11.1	c	1028	0.011	17	0.60	1.7	0.51	18	83	183	377	76	10	197	0.28	25.4
12.1	om	293	0.007	8	0.18	0.5	0.20	5	23	52	124	26	11	195	0.39	32.0
Sample CD-22D																
1.1	c	1397	0.024	22	1.00	3.5	1.01	36	138	243	385		10	128	0.27	12.9
2.1	om	731	0.015	18	0.49	1.5	0.42	16	73	135	238		11	183	0.26	18.3
3.1	c	581	0.027	11	0.36	1.1	0.27	12	58	114	212		11	85	0.23	21.5
4.1	om	985	0.016	17	0.43	1.6	0.29	19	94	188	344		12	178	0.16	22.2
5.1	c	1272	0.040	14	0.99	3.5	0.95	35	134	230	368		10	60	0.26	12.8
6.1	c	471	0.022	14	0.44	1.1	0.25	11	44	80	140		10	113	0.22	15.2
7.1	r	1522	0.186	66	1.44	3.4	1.09	32	144	286	507		10	87	0.32	19.2
7.2	c	1279	0.054	24	1.52	3.5	0.98	32	132	234	388		10	70	0.28	14.6
8.1	om	1042	0.023	22	0.83	2.4	0.60	24	104	195	331		11	143	0.24	16.8
9.1	c	1563	1.32	62	3.80	5.3	1.40	37	168	295	508		12	16	0.31	16.7
9.2	r	5168	16.70	363	57.4	47.3	19.99	208	665	814	1303		11	7	0.61	7.6
10.1	c	1991	0.045	14	3.61	7.4	2.06	61	217	355	551		9	34	0.29	11.0
11.1	c	1382	0.018	14	1.02	2.9	0.72	31	134	253	451		12	93	0.23	17.7
12.1	c	1316	0.026	18	1.18	3.3	0.94	33	135	246	420		11	97	0.28	15.6
13.1	c	1178	0.020	11	1.44	3.7	1.20	34	130	215	352		11	65	0.33	12.6
14.1	om	877	0.034	24	0.56	1.5	0.39	16	77	166	357		13	135	0.24	27.5
15.1	c	1264	2.05	142	7.02	7.2	2.95	38	143	227	382		12	22	0.54	12.1
16.1	c	1161	0.023	14	1.20	2.8	0.76	26	119	226	402		11	78	0.27	18.8
Sample CD-7D																
1.1	om	3379	0.123	65	7.33	14.9	6.24	112	372	599	971		9	66	0.46	10.5
2.1	om	1291	0.593	20	3.25	3.8	1.52	30	125	242	437		9	9	0.43	17.7
2.2	c	1336	1.09	63	12.4	10.2	5.28	39	132	242	504		12	12	0.80	15.5
3.1	r	27359	0.112	5398	1096	715	562.16	2744	4731	3703	4511		14	1089	1.22	2.0
3.2	c	1029	0.055	15	0.80	2.2	0.47	23	104	193	334		11	54	0.20	17.3
4.1	r	8112	35.6	960	226	151	104.05	500	1016	1191	2053		13	7	1.15	5.0
5.1	om	1458	0.668	44	6.98	8.1	3.24	49	157	250	415		12	15	0.49	10.3
6.1	r	16228	131	1668	252	151	61.84	612	2439	3388	6434		17	5	0.62	12.7
6.2	c	1311	0.341	31	2.95	4.9	2.81	35	127	237	469		8	22	0.65	16.0
7.1	om	3844	9.28	245	59.2	47.1	27.87	189	465	543	774		10	7	0.90	4.9
8.1	om	874	0.668	32	1.82	2.7	1.02	22	87	160	277		10	17	0.40	15.0
9.1	c	2258	1.06	82	8.04	12.0	5.37	82	260	393	624		7	19	0.52	9.1
10.1	r	5041	22.5	600	126	83.9	54.90	285	649	761	1222		11	7	1.08	5.2
10.2	om	2367	2.32	44	12.7	11.1	5.13	60	239	425	778		12	5	0.60	15.6
11.1	om	1259	0.055	23	1.23	2.0	1.18	19	99	227	503		7	71	0.59	32.8
Sample CD-8D																
1.1	c	1583	0.086	33	5.63	8.8	5.70	57	163	267	468		8	46	0.77	9.9
2.1	c	1479	0.046	27	3.65	6.6	3.54	47	151	256	448		9	66	0.61	11.6
3.1	om	2299	0.084	83	0.77	2.3	0.98	31	186	434	893		13	229	0.35	34.5
4.1	c	450	0.131	8	0.41	0.6	0.20	6	37	87	197		13	21	0.31	40.6
5.1	om	754	0.019	10	0.76	1.8	0.47	18	77	139	245		10	74	0.25	16.3
6.1	c	786	0.714	41	2.38	2.4	1.12	19	75	143	272		10	19	0.51	17.4
7.1	c	2579	0.043	97	2.51	5.6	2.91	53	231	461	852		10	280	0.51	19.4
8.1	c	1206	0.213	25	2.41	4.6	2.56	35	123	217	404		8	25	0.61	13.8
9.1	om	1556	0.027	57	1.05	2.7	1.62	28	131	289	576		10	305	0.57	25.1
10.1	c	2103	0.072	44	5.10	8.8	4.80	67	215	371	666		9	72	0.60	12.1
11.1	c	568	0.124	17	0.95	1.6	0.81	13	54	103	204		6	34	0.54	18.5
12.1	c	779	0.030	16	1.06	2.3	1.35	19	76	143	277		9	79	0.62	17.3
13.1	c	1191	0.087	36	3.68	6.3	3.54	43	127	204	353		9	57	0.65	9.8
14.1	c	1536	0.024	45	2.26	5.4	2.62	43	154	270	482		11	198	0.52	13.4
15.1	c	1983	0.103	56	4.71	8.8	4.19	64	208	351	594		10	73	0.54	11.2
16.1	om	1087	0.058	27	1.04	2.4	1.41	22	96	199	399		8	87	0.59	21.8

Note: All analyses were performed on the sensitive high-resolution ion microprobe—reverse geometry (SHRIMP-RG) at the U.S. Geological Survey—Stanford University Microanalytical Center, Stanford, California, following procedures outlined in Mazdab and Wooden (2006). All abundances are expressed in ppm.

[†]Spot labeled as grain number.spot number. Cathodoluminescence (CL) designations: om—oscillatory zoned mantle; c—core; r—rim.

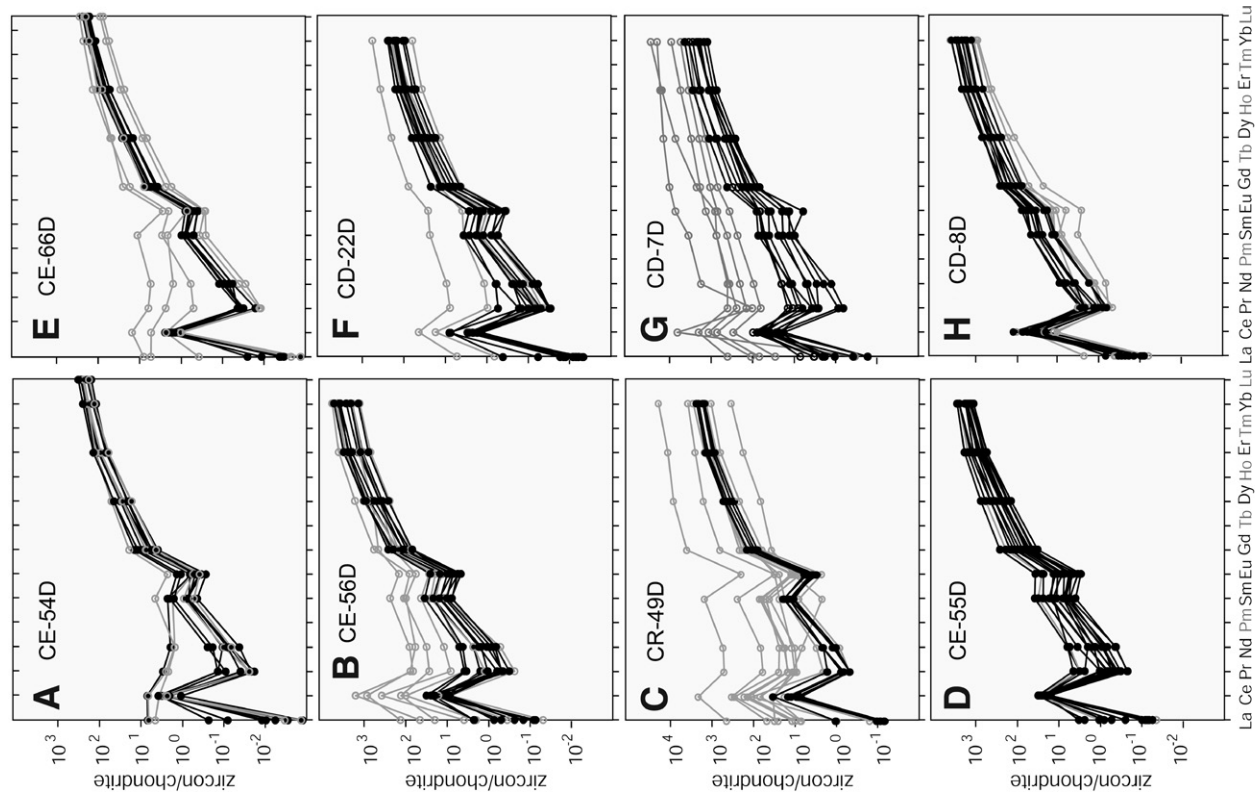


Figure 8. Chondrite-normalized trace-element plots of the analyzed zircons from the samples treated in this study (see text for further explanations; for data sources, see Table 2).

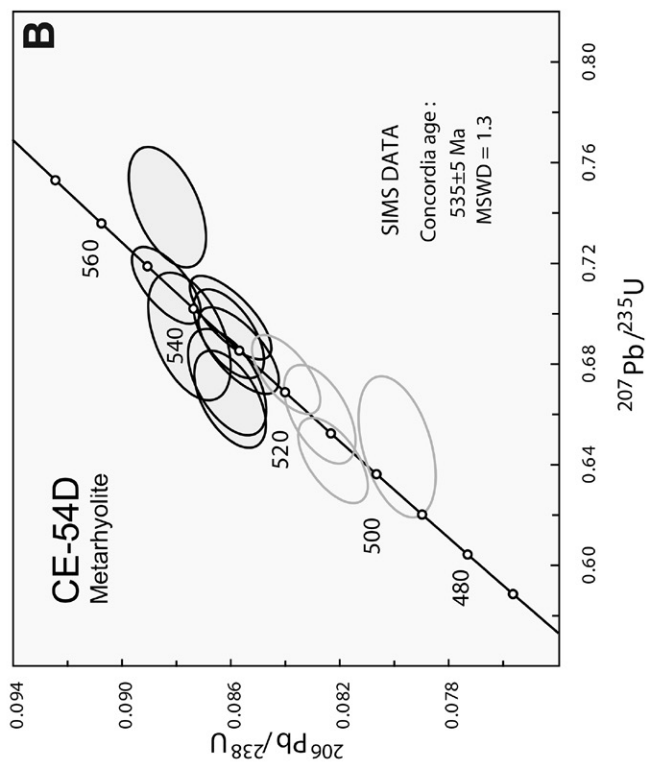
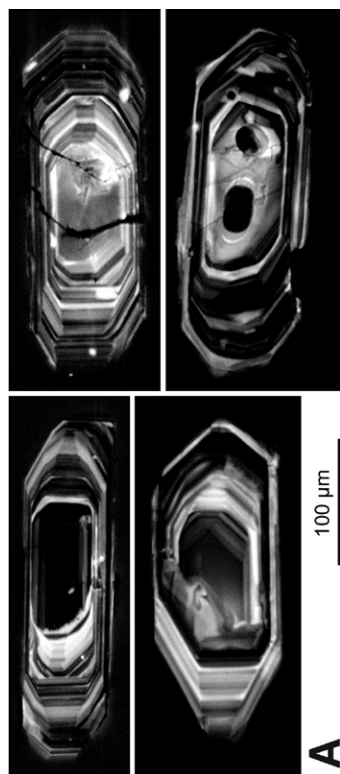


Figure 7. Metarhyolite from the northern part of the Agua del Rio occurrence (sample CE-54D; for location, see Fig. 3A). (A) Representative cathodoluminescence photomicrographs of zircons. They show oscillating growth textures (top) and partly also cores, opaque inclusions, and corrosion (bottom). (B) Concordia diagram of secondary ionization mass spectrometry (SIMS) data. Light-gray ellipses represent analyses not used in the calculation. MSWD—mean square of weighted deviates.

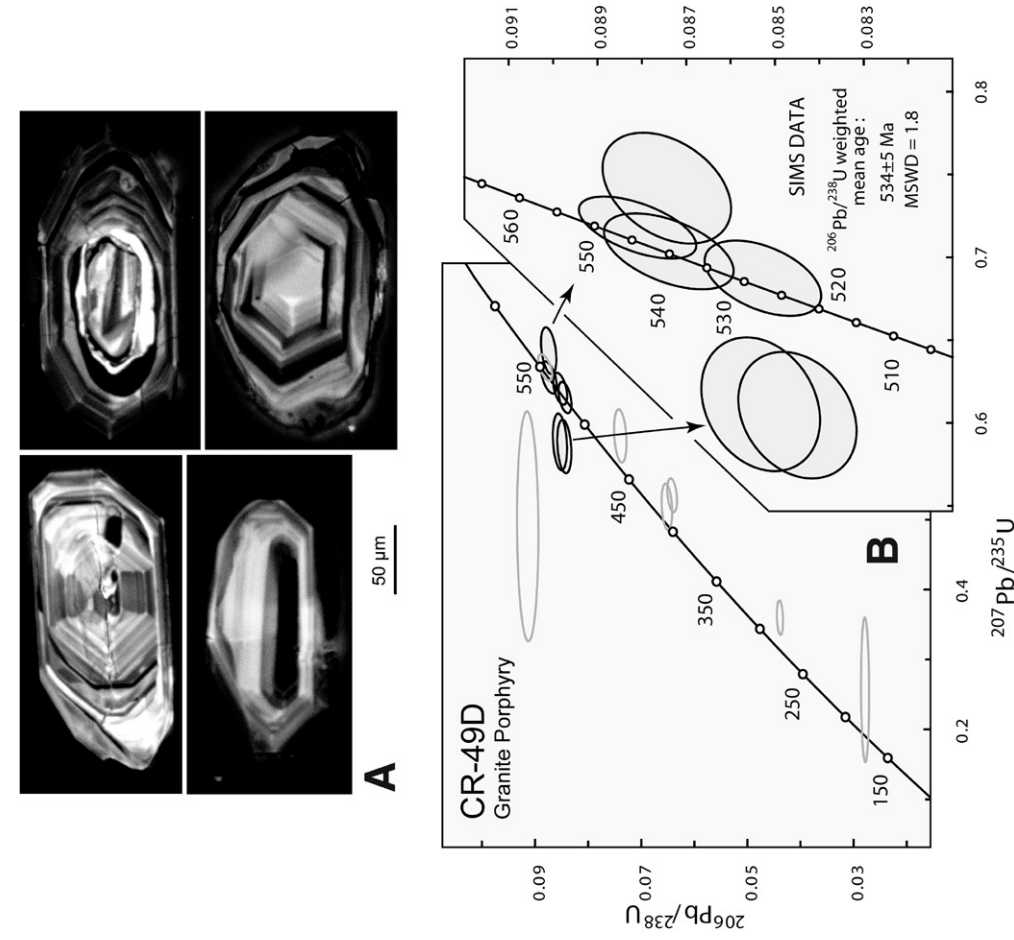


Figure 10. Granite porphyry (sample CR-49D) from the area south of San Pedro Norte, west of Estancia Sacha Corral; for location, see Figure 4. (A) Zircons in representative cathodoluminescence photographs either record an oscillating growth (top left), rarely contain older cores (top right), or show diffuse patterns (bottom). (B) Concordia diagram of secondary ionization mass spectrometry (SIMS) data. Light-gray ellipses represent analyses not used in the calculation. MSWD—mean square of weighted deviates.

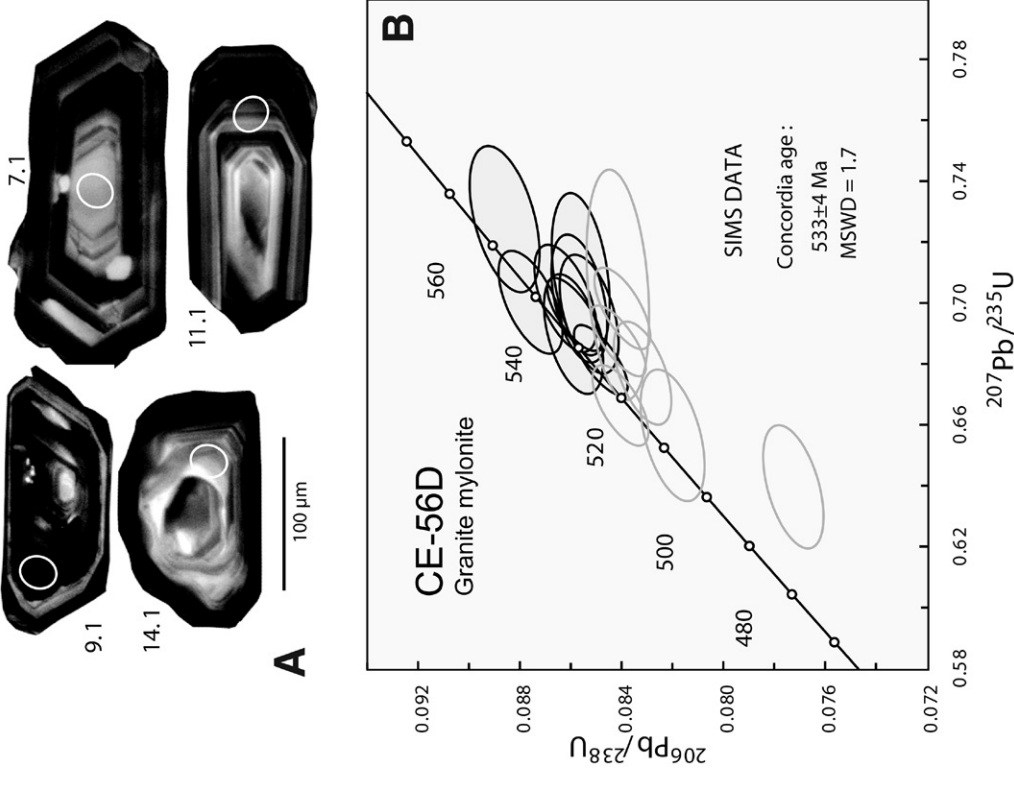


Figure 9. Talayaco granite mylonite (sample CE-56D) from the Talayaco occurrence; for location, see Figure 3B. (A) Representative cathodoluminescence photographs of zircons. Ellipses indicate sensitive high-resolution ion microprobe–reverse geometry (SHRIMP-RG) U–Pb and trace-element analysis spots labeled by grain number and spot number. (B) Concordia diagram of secondary ionization mass spectrometry (SIMS) data. Light-gray ellipses represent analyses not used in the calculation. MSWD—mean square of weighted deviates.

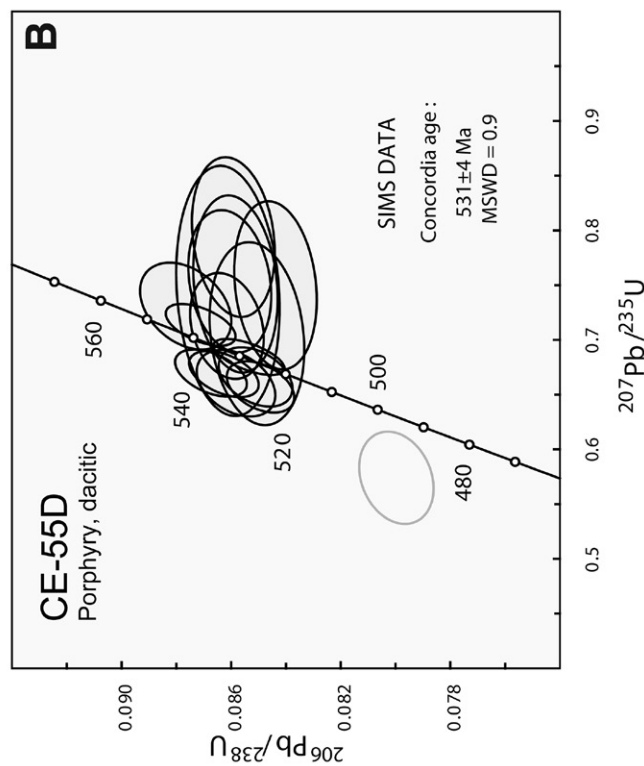
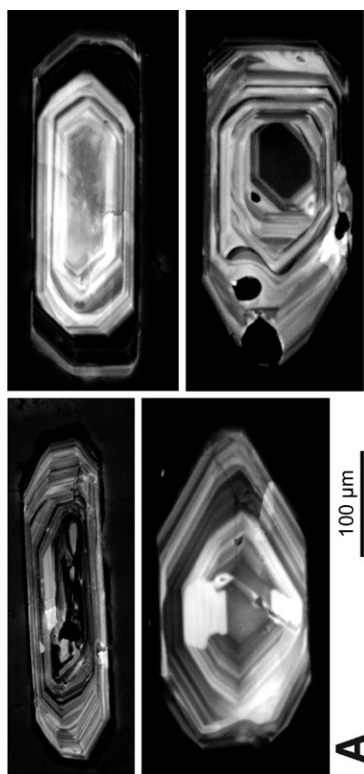


Figure 11. Dacitic porphyry (sample CE-55D) from the western part of the Agua del Rio occurrence; for location, see Figure 3A. (A) Representative cathodoluminescence photographs of zircon. The magmatic grains record an oscillating growth (top), partly contain inclusions but no cores (top right), and can be corroded (bottom right). (B) Concordia diagram of secondary ionization mass spectrometry (SIMS) data. Light-gray ellipse represents an analysis not used in the calculation. MSWD—mean square of weighted deviates.

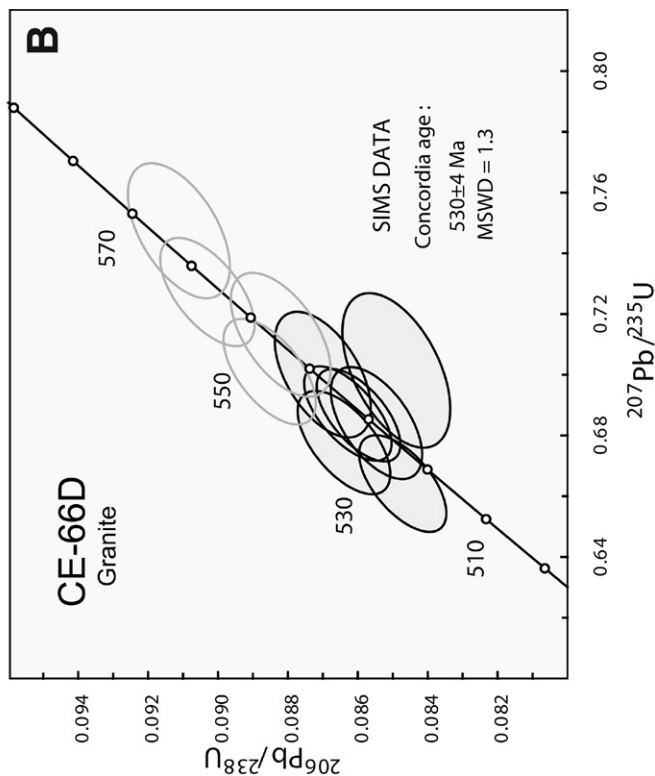
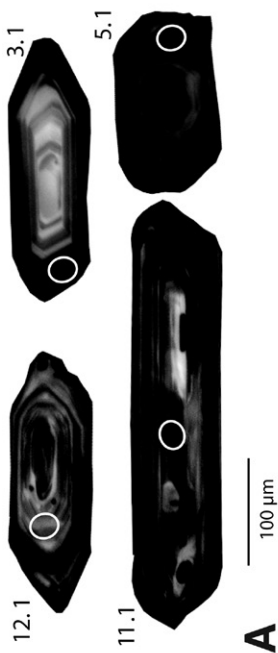


Figure 12. El Tio granite (sample CE-66D; for location, see Fig. 5B). (A) Representative cathodoluminescence photographs of zircon. Ellipses indicate sensitive high-resolution ion microprobe–reverse geometry (SHRIMP-RG) U-Pb and trace-element analysis spots labeled by grain number, spot number. (B) Concordia diagram of secondary ionization mass spectrometry (SIMS) data. Light-gray ellipses represent analyses not used in the calculation. MSWD—mean square of weighted deviates.

evidence for inherited cores. TIMS analyses of single grains indicate clear Pb loss. LREE patterns for three grains analyzed by SIMS show variability (Fig. 8E), indicating disturbance of the systematics. Excluding the four oldest analyses and one obviously disturbed analysis, the remaining seven give a concordia age of 530 ± 4 Ma (Fig. 12B), which is interpreted as the crystallization age of the zircons. The older rejected analyses are interpreted to represent slightly older xenocrystic cores, assuming the U-Pb systematics have not been disturbed.

Subequant to elongate oscillatory zoned zircons from the Rodeito rhyolite to dacite (CD-22D; Fig. 13A) give a range of discordant to concordant analyses that result from the combined effects of inheritance and Pb loss. Several analyses have elevated LREE patterns (Fig. 8F), but the analyses are overall consistent with one another and do not vary as a function of U-Pb age. Excluding older ages assumed to reflect inheritance and younger ages attributed to Pb loss, 10 of 18 analyses give a concordia age of 523 ± 5 Ma (Fig. 13B), which is interpreted to reflect the age of crystallization of the zircons.

The sample from the El Escondido rhyolite (CD-7D) contains clear colorless, oscillatory zoned zircons with minor inclusions (Fig. 14A). Five analyses of higher-U core and rim portions of the grains give discordant results with younger $^{206}\text{Pb}/^{238}\text{U}$ ages and elevated LREE patterns (Fig. 8G). Rejecting an additional three analyses with slightly younger $^{206}\text{Pb}/^{238}\text{U}$ ages but relatively undisturbed REE spectra compared to the concordant analyses, the remaining seven analyses define a concordia age of 519 ± 4 Ma (Fig. 14B).

The El Escondido granite (CD-8D) contains a heterogeneous population of colorless to yellow-brown, elongate to equant, euhedral zircons. The grains typically have cores mantled by oscillatory zoned zircon (Fig. 15A). SIMS analyses yield $^{206}\text{Pb}/^{238}\text{U}$ ages ranging from 470 to 544 Ma. The four oldest ages are from domains that differ in REE pattern with slightly lower middle REE abundances (Fig. 8H). Excluding these four analyses as inherited xenocrysts and the two youngest analyses that record Pb loss, the remaining 10 give a $^{206}\text{Pb}/^{238}\text{U}$ weighted mean age of 521 ± 4 Ma (Fig. 15B).

INTERPRETATION

The crystallization age of 535 ± 5 Ma for the rhyolite at Agua del Río (CE-54D) suggests an Early Cambrian (Terreneuvian) age (time scale of Walker et al., 2012) for this part of the clastic succession with intercalated rhyolite to rhyodacite layers. The new age is within uncertainty of a K-Ar whole-rock date of 527 ± 21 Ma from a

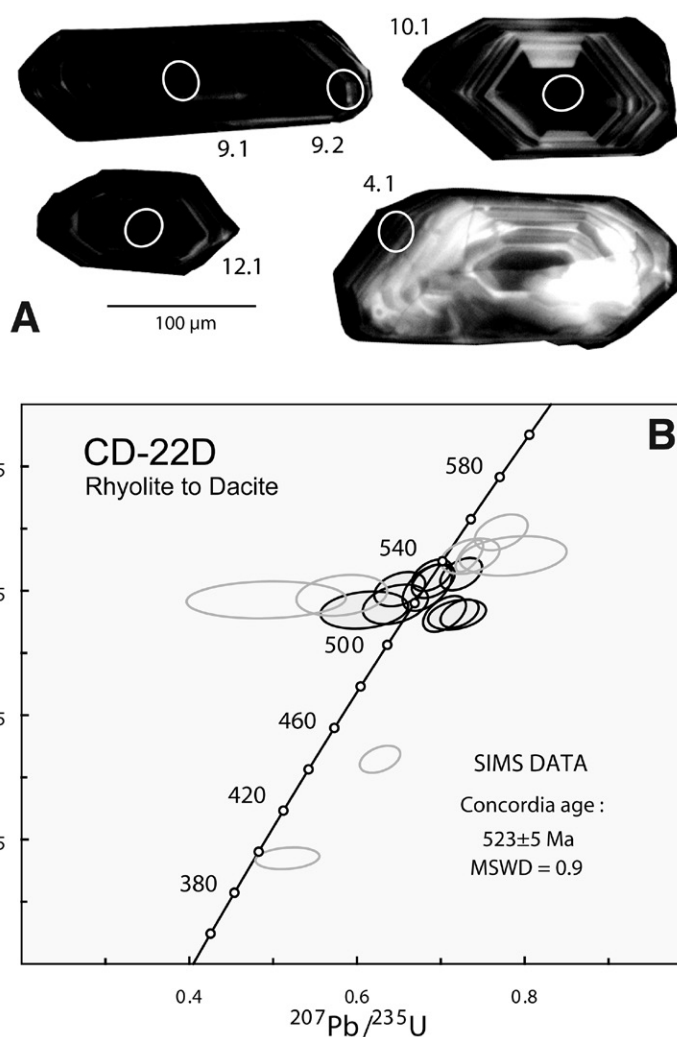


Figure 13. Rodeito rhyolite to dacite (sample CD-22D; for location, see Fig. 5A). (A) Representative cathodoluminescence photographs of zircons. Ellipses indicate sensitive high-resolution ion microprobe–reverse geometry (SHRIMP-RG) U-Pb and trace-element analysis spots labeled by grain number, spot number. (B) Concordia diagram of secondary ionization mass spectrometry (SIMS) data. Light-gray ellipses represent analyses not used in the calculation. MSWD—mean square of weighted deviates.

rhyolitic porphyry in the La Lidia area (Massabie et al., 2002). Combining the SIMS age with the older conventional U-Pb zircon age from the basal rhyolite that is overlain by the clastic succession in the La Lidia area to the south ($584 +22/-14$ Ma; Llambías et al., 2003) and the 560 Ma detrital zircon age (U-Pb, SIMS), indicating the maximum age of deposition in the southernmost part of the Sierra Norte (Iannizzotto et al., 2013), suggests that sedimentary deposits along with the underlying and intercalated acid volcanic rocks are Neoproterozoic to Early Cambrian in age.

The SIMS age of 534 ± 5 Ma for the synkinematic granite porphyry that intruded the dextral mylonite zone south of San Pedro Norte

(CR-49D), interpreted as the age of crystallization, provides a time marker for the age of dextral shearing and mylonitization in this part of the Sierra Norte area related to the second stage of the Pampean deformation (D_2). It falls in the time span of dextral mylonitization in the southernmost part of the Sierra Norte found by Iannizzotto et al. (2011, 2013).

The 533 ± 4 Ma SIMS age from the granite mylonite of Talayaco (CE-56D) is interpreted as the crystallization age of the protolith. This date also provides a lower age limit of sedimentation in this part of the Sierra Norte, since the granite intruded the section, and an upper age limit of D_2 mylonitization, since the granite is deformed. This age is older than the 531 ± 4 Ma SIMS date

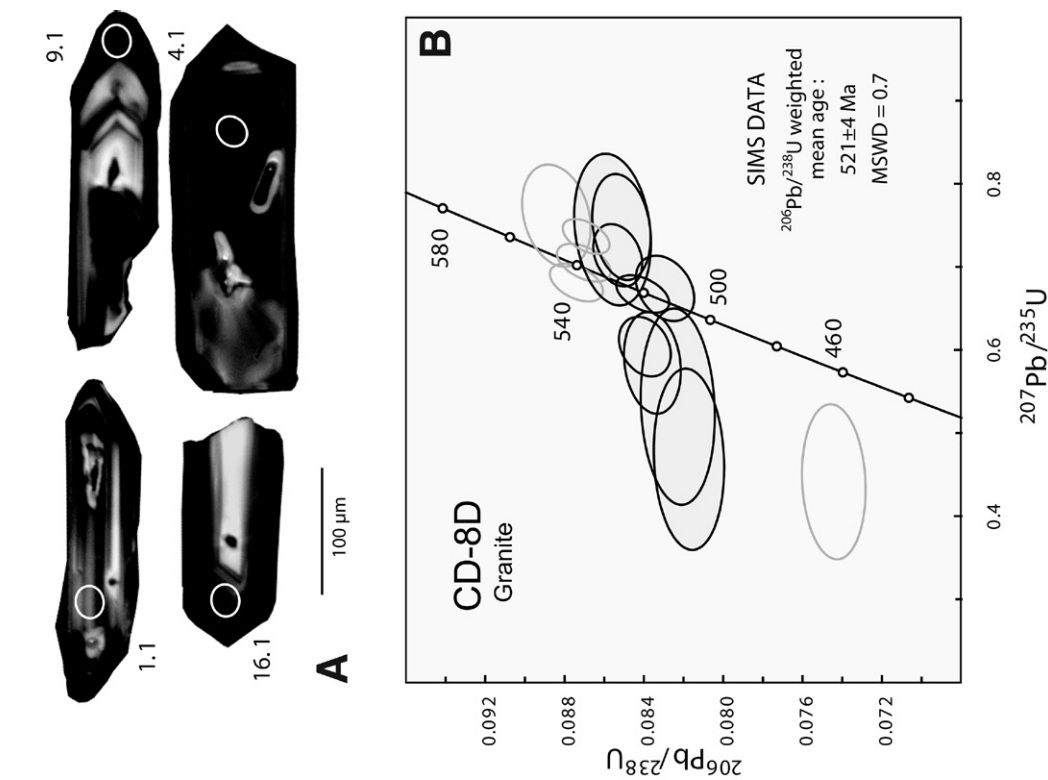


Figure 15. El Escondido granite (sample CD-8D) from the El Escondido occurrence west of Villa Ojo de Agua (Santiago del Estero Province; for location, see Fig. 5C). (A) Representative cathodoluminescence photographs of zircons. Ellipses indicate sensitive high-resolution ion microprobe-reverse geometry (SHRIMP-RG) U-Pb and trace-element analysis spots labeled by grain number, spot number. (B) Concordia diagram of secondary ionization mass spectrometry (SIMS) data. Light-gray ellipses represent analyses not used in the calculation. MSWD—mean square of weighted deviates.

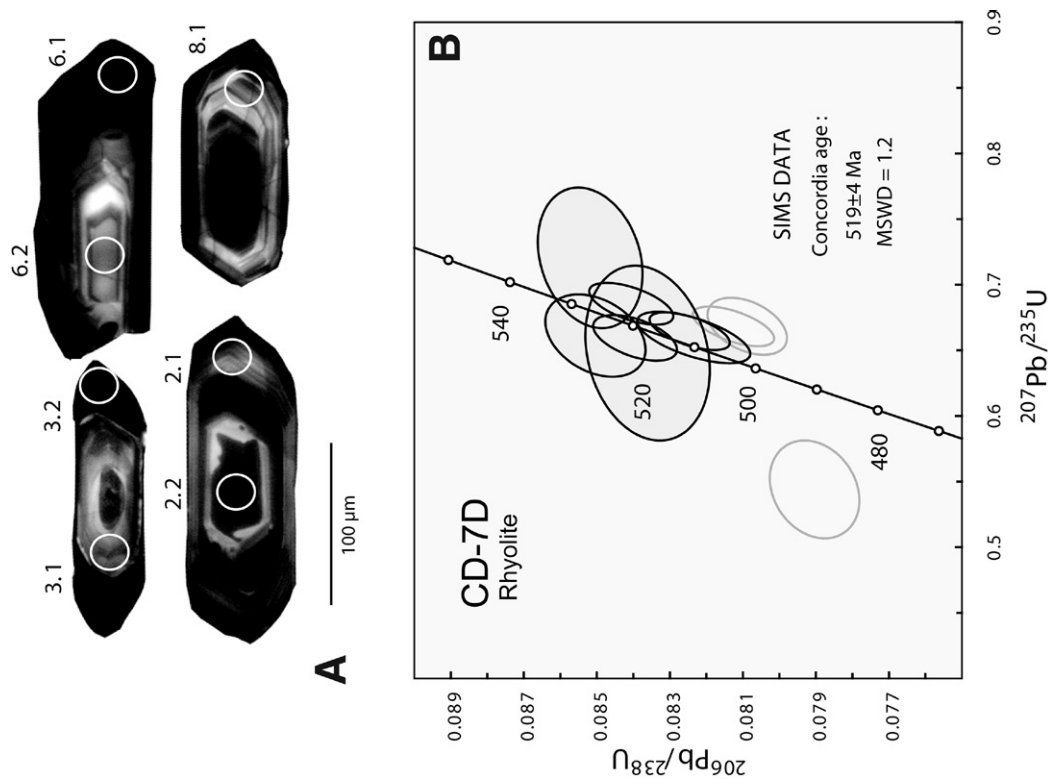


Figure 14. El Escondido rhyolite (sample CD-7D) from the El Escondido occurrence west of Villa Ojo de Agua (Santiago del Estero Province; for location, see Fig. 5C). (A) Representative cathodoluminescence photographs of zircons. Ellipses indicate sensitive high-resolution ion microprobe-reverse geometry (SHRIMP-RG) U-Pb and trace-element analysis spots labeled by grain number, spot number. (B) Concordia diagram of secondary ionization mass spectrometry (SIMS) data. Light-gray ellipses represent analyses not used in the calculation. MSWD—mean square of weighted deviates.

from the dacitic porphyry of Agua del Río (CE-55D), which we interpret as the age of crystallization for this sample. It provides the approximate timing of the final stage of compressive Pampean D_2 deformation.

The SIMS zircon date of 530 ± 4 Ma from the postkinematic El Tío granite (CE-66D) suggests that the intrusion is not part of the undeformed Cambrian Ambargasta granite pluton (Figs. 5B and 6), the age of which was broadly estimated in the La Clemira area by K-Ar biotite dates of 517 ± 15 and 500 ± 15 Ma (Castellote, 1982). The SIMS date suggests that compressive deformation and regional metamorphism of the clastic rocks in the Sierra Norte area (La Lidia–Simbol Huasi Formation) should be Early Cambrian in age. The results presented here broadly point to a time span between 535 ± 5 and 530 ± 4 Ma for the first and second Pampean compressive deformation events (D_1 , D_2), accompanying regional metamorphism, and subsequent uplift in the Sierra Norte de Córdoba. This time span is similar to that obtained by Iannizzotto et al. (2013) from the southernmost part of the Sierra Norte. The narrow age range is consistent with the SIMS dates of 519 ± 4 Ma from the undeformed El Escondido rhyolite (CD-7D) and 523 ± 5 Ma from the Rodeito rhyolite to dacite (CD-22D), both interpreted as reflecting the age of crystallization of igneous rocks that record acid magmatism after clastic sedimentation and cessation of the D_2 deformation in the Sierra Norte de Córdoba.

The El Escondido granite (CD-8D), with an interpreted emplacement age of 521 ± 4 Ma (SIMS), records late-stage Pampean magmatism. Overlying clastic rocks of the El Escondido Formation can be estimated to be mid-Cambrian or younger in age. The lack of deformation of the El Escondido granite indicates that no ductile deformation has taken place during Middle Cambrian–Ordovician and later times. Thus, Pampean deformation and metamorphism terminated before the Middle Cambrian, and this area was not affected by later Famatinian compression and regional metamorphism. The slightly deformed Ojo de Agua granite to the east, however, yielded a late Early Cambrian age (515 ± 4 Ma, U-Pb, zircon, SIMS; Stuart-Smith et al., 1999), suggesting that Pampean deformation may have locally persisted into Middle Cambrian time.

The SIMS date from the Rodeito rhyolite to dacite (CD-22D) is older than the age of the Los Burros dacite that intruded the eastern part of the Rodeito occurrence of clastic metasedimentary rocks (Fig. 5A). In the Totorillas area, the undeformed Los Burros dacite has been shown to be lowermost Middle Cambrian in age (512.6 ± 3.5 Ma; U-Pb, zircon, SIMS; Leal et

al., 2003), which gives a further constraint for the lower time limit of the Pampean deformational history.

MODEL OF PAMPEAN EVOLUTION AT THE WESTERN PRE-ANDEAN GONDWANA MARGIN

The isotopic dates provide additional time constraints for the different stages of the sedimentary, tectonic, and magmatic evolution in this easternmost segment of the Eastern Sierras Pampeanas and provide a more robust interpretation of the tectonic evolution of the pre-Andean Gondwana margin. Our present interpretation partly modifies those given by Rapela et al. (2007), von Gosen and Prozzi (2010), Casquet et al. (2012), and Iannizzotto et al. (2013). The isotopic dates presented here partly overlap in the range of errors, reflecting the complex systematics of the zircons as defined by both the TIMS and SIMS data. Use of both techniques enhances the characterization of zircon systematics and strengthens the reliability of the interpreted crystallization ages. Additional chemical-abrasion-TIMS analysis (Mattinson, 2005) of grains screened for simple systematics is an obvious next step in further refining the timing of magmatism and deformation in this setting. Nevertheless, we interpret the chronological succession of different events as follows (compare interpretative chart of Fig. 16 and diagrams of Fig. 17). The geographic orientations cited refer to present coordinates.

Sedimentation (Ediacaran–Early Cambrian)

The time interval of deposition of the clastic sediments in the Sierra Norte de Córdoba is constrained by two isotopic dates. Detrital zircons from metasedimentary rocks in the southernmost Sierra Norte have a minor peak at 560 Ma defined by individual ages ranging from 537 ± 9 Ma to 570 ± 7 Ma (Iannizzotto et al., 2013). Considering the unresolved potential for Pb loss to skew the detrital zircon ages to younger ages, these results broadly limit the time of deposition to younger than ca. 560 Ma. Given this uncertainty, the detrital data are consistent with the greater age of $584 +22/-14$ Ma reported by Llambías et al. (2003) from the basal meta-rhyolite (ignimbrite) beneath the clastic succession in the La Lidia area. Additional high-precision data are needed to further refine limits on the depositional age of these units.

The new crystallization (SIMS) age of 535 ± 5 Ma for the intercalated and deformed meta-rhyolite at Agua del Río suggests that cessation of sedimentation and the onset of D_1 deformation took place sometime after this date. The

intrusion of the later mylonitized Talayaco granite (533 ± 4 Ma, SIMS, crystallization age) into the clastic deposits provides an additional approximate time marker in the Early Cambrian. However, the precise lower age limit of clastic sedimentation remains uncertain. These ages, combined with the loose constraint provided by Iannizzotto et al. (2013), suggest that deposition of the clastic sediments and acid magmatism in the Sierra Norte area took place in the Ediacaran–Early Cambrian interval. Thus, the metasedimentary rocks are time equivalents and represent the southern continuation of the Puncoviscana Formation (*sensu lato*) of northwest Argentina (see introductory section).

The clastic deposits in the Sierra Norte are characterized by metaconglomerates and fine-grained metaclastic rocks with intercalated meta-rhyolites and metadacites. The clastic deposits include locally derived detritus of clastic, magmatic, and metamorphic rocks with paleocurrent indicators indicating an approximately west-directed sedimentary transport (von Gosen and Prozzi, 2009, with further information therein). Geochemical analysis of clastic metasedimentary rocks shows that those from the Sierra Norte de Córdoba were deposited in a passive-margin setting, whereas those from the Sierras de Córdoba and Sierra de Guasayán point to an active arc setting (von Gosen et al., 2009).

Observations from the clastic succession in the Sierra Norte combined with the presence of acid magmatism suggest a postrift passive-margin setting for the sequence (von Gosen and Prozzi, 2009, 2010; von Gosen et al., 2009). Although geochemical data from the intercalated magmatic rocks do not exist, we interpret the magmatism as extension-related prior to emplacement of the arc intrusions (see following). The precise configuration of the margin remains uncertain.

It is unclear whether and to what extent the clastic sequence is underlain by basement rocks because rocks with a clear Proterozoic age are still not known from the Sierra Norte area. The only possible candidate is the Pozo del Macho Formation (compare Martino and Guerreschi, 2004). At least one deformation event and regional metamorphism of these mica schists and gneisses and equivalent rocks in the south-east (Fig. 6) may be Neoproterozoic in age. This is consistent with the interpretation of Martino and Guerreschi (2004) and two K-Ar whole-rock dates of Castellote (1985b). If such an age is confirmed by later studies, then these rocks may represent part of the Proterozoic “basement” below the La Lidia–Simbol Huasi Formation (Fig. 16).

Our interpretation of a west-facing passive margin (Fig. 17A) during the Ediacaran–Early Cambrian interval is comparable with that of

	Lithological Units and Events	Igneous Rocks	Isotopic Dating
Ordovician			
		Oncán Porphyries	483±14 Ma, K-Ar, whole rock: (6) 494±11 Ma, Rb-Sr: (3)
Furongian			
			Hornfels: 500±14 Ma, K-Ar, whole rock: (4)
Epoch 3	contact metamorphism	Ambargasta granite	517±15 Ma, 500±15 Ma, K-Ar, biotite: (1)
	uplift	Los Burros dacite Dacitic dykes	512.6±3.5 Ma, U-Pb, zircon, SIMS: (8) El Escondido: 514±15 Ma, K-Ar, whole rock: (7)
Epoch 2	local shearing (age unclear)	Ojo de Agua granite	515±4 Ma, U-Pb, zircon, SIMS: (5)
	uplift	Rhyolite El Escondido granite Rhyolite to Dacite	El Escondido: 519±4 Ma, U-Pb, zircon, SIMS 521±4 Ma, U-Pb, zircon, SIMS Rodeito: 523±5 Ma, U-Pb, zircon, SIMS
Cambrian	contact metamorphism	El Tío granite Villa Albertina granite	530±4 Ma, U-Pb, zircon, SIMS 530±4 Ma, U-Pb, zircon, SIMS: (12)
	uplift		
Terreneuvian	D ₂ -deformation and metamorphism (dextral shearing and mylonitization)	Porphyry, dacitic Granodiorite-Monzogranite San Miguel gneiss Talayaco granite Granite Porphyry	Agua del Río: 531±4 Ma, U-Pb, zircon, SIMS Miarolitic Monzogranite: 531±27 Ma, U-Pb, zircon: (10) Granodiorite: 532±8 Ma, U-Pb, zircon: (10) 533±12 Ma, U-Pb, zircon, SIMS: (11) 533±4 Ma, U-Pb, zircon, SIMS 534±5 Ma, U-Pb, zircon, SIMS
	D ₁ -deformation and regional metamorphism		
Ediacaran	Clastic succession with acid magmatic rocks (La Lidia-Símbol Huasi Formation s.l.) ? ?	Rhyolite ← Dacite Granodiorite Monzogranite	Agua del Río, metarhyolite: 535±5 Ma, U-Pb, zircon, SIMS Porphyritic dacite: 535±8 Ma, U-Pb, zircon: (10) Juan García granodiorite: 537±4 Ma, U-Pb, zircon, SIMS: (12) Lineated granodiorite: ~540 Ma, U-Pb, zircon: (10) Monzogranite: 542±11 Ma, U-Pb, zircon: (10) Monzogranite: 554±7 Ma, U-Pb, zircon: (10) Quartzite gneiss: 560 Ma, U-Pb, detrital zircons, SIMS, max. age for sedimentary deposition of protolith: (12) 567±16 Ma, K-Ar, whole rock: (4)
	? compressive deformation and metamorphism	Rhyolite ←	Metarhyolite (ignimbrite): 584+22/-14 Ma, U-Pb, zircon: (9)
Cryogenian	Pozo del Macho Formation and equivalents	←	665±20 Ma, 612±20 Ma, K-Ar, whole rock: (2)
	underlying rocks unknown		

Figure 16. Interpretation of the different stages of the evolution of the Sierra Norte de Córdoba and adjacent parts of the Santiago del Estero Province (simplified and schematic chart), based on von Gosen and Prozzi (2010), isotopic dates of the present study, and dates from (1) Castellote (1982), (2) Castellote (1985b), (3) Rapela et al. (1991), (4) Koukharsky et al. (1999), (5) Stuart-Smith et al. (1999), (6) Correa (2003), (7) Koukharsky et al. (2003), (8) Leal et al. (2003), (9) Llambías et al. (2003), (10) Schwartz et al. (2008), (11) Siegesmund et al. (2010), and (12) Iannizzotto et al. (2013). The left column is based on the time scale of Walker et al. (2012). SIMS— secondary ion mass spectrometry.

Schwartz et al. (2008), although they proposed a Neoproterozoic age. This contrasts to models of Rapela et al. (2007) and Iannizzotto et al. (2013), who postulated a forearc setting and to that of Siegesmund et al. (2010), who proposed deposition in arc-related basins. The passive-

margin interpretation, however, is similar to the geotectonic model of Casquet et al. (2012). These authors do not exclude a passive-margin setting for the older part of the Puncoviscana Formation on the western margin of the Kalahari craton with the Clymene Ocean in the west

(their Fig. 4). Based on Cordani et al. (2013), we think that the Sierra Norte passive margin faced westward to the Puncoviscana Ocean of Escayola et al. (2011), and clastic sediments were shed from the east into this depocenter (Puncoviscana tract of Escayola et al., 2011).

Subduction and D₁ Deformation (Early Cambrian)

In conjunction with the other isotopic dates (see following), the previously presented Early Cambrian ages are time markers for the compressive D₁ deformation and accompanying regional metamorphism of the clastic metasedimentary succession in the Sierra Norte de Córdoba. Deformation led to the formation of large-scale anticlines and synclines accompanied by an S₁ cleavage.

The D₁ deformation in the Early Cambrian (Fig. 16), interpreted as the result of partitioned dextral transpression (von Gosen and Prozzi, 2010), probably was related to east- to north-east-directed subduction with the Sierra Norte de Córdoba representing the upper plate on the Gondwanan side (von Gosen and Prozzi, 2010) and the accretionary complex developing in the southwestern and western footwall (e.g., Northrup et al., 1998; Fig. 17B herein). Oblique subduction was also proposed by Rapela et al. (2007) and Iannizzotto et al. (2013). According to Rapela et al. (1998a), it seems that compressive deformation led to the destruction of the passive margin. The mechanism operating during this change from passive to active margin, however, is unclear. It is possible that subduction initiation along the margin was preceded and localized by a strike-slip fault.

Geochemical analyses in the central part of the Sierra Norte area have shown that the granitoid intrusions of the Sierra Norte–Ambargasta batholith are products of a precollisional active continental margin forming a calc-alkaline magmatic arc (e.g., Lira et al., 1997). This is supported by geochemical analyses in the southern part of the Sierra Norte (Iannizzotto et al., 2013). We propose that the magmatic arc formed in the former passive-margin segment now representing the upper plate (compare Figs. 17A and 17B).

The timing of the onset of subduction is not well constrained. U-Pb zircon dates (TIMS) of two intrusions in the Sierra Norte reported by Schwartz et al. (2008; Fig. 16 herein) suggest subduction was on going by ca. 555 Ma. In this scenario, clastic sedimentation in the developing accretionary complex was coeval with intrusive activity in the eastern upper plate. Compressive D₁ deformation in the newly formed arc then may have begun prior to the Early Cambrian

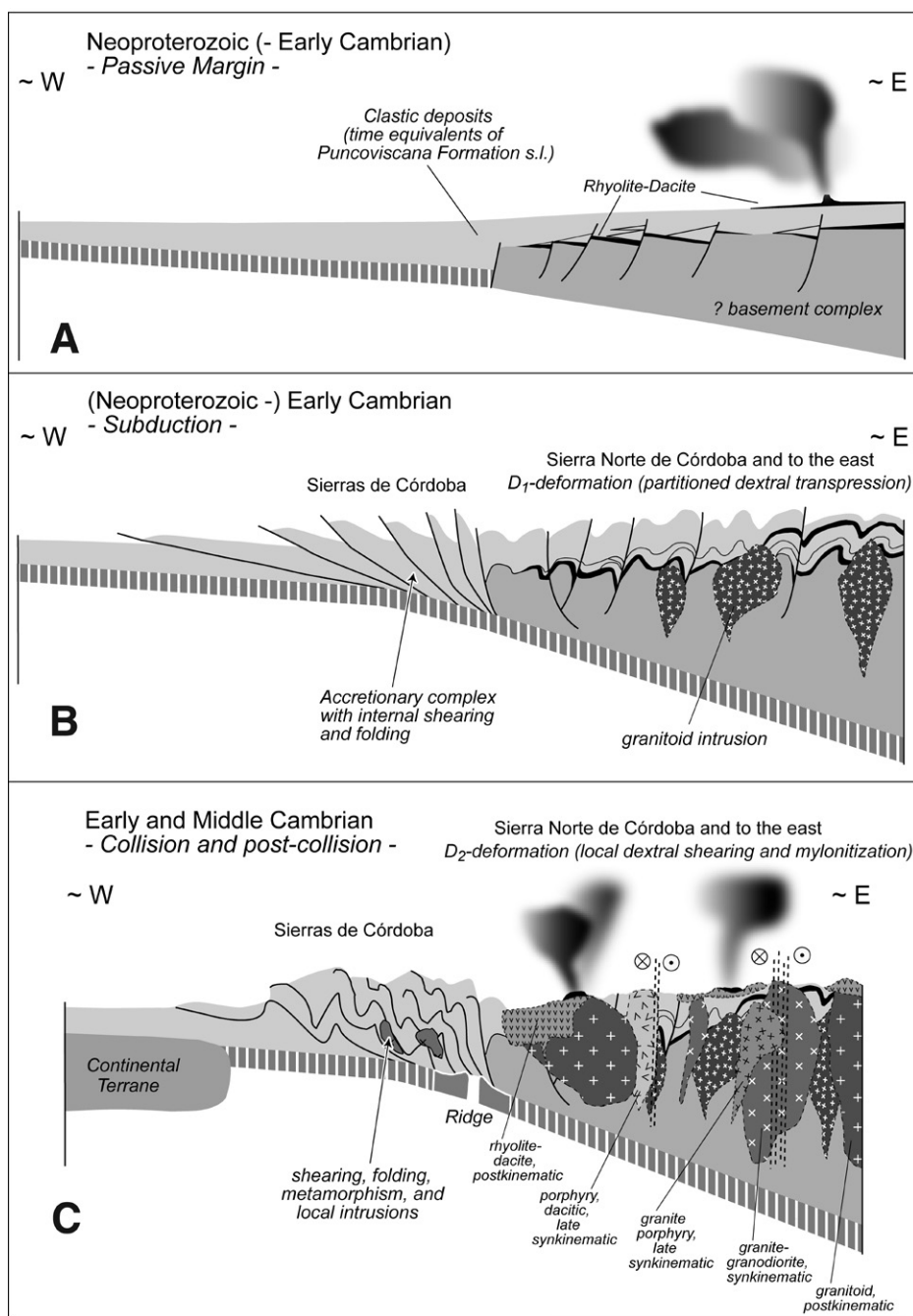


Figure 17. Schematic, simplified, and composite profile cartoons (not to scale) to illustrate the interpreted different stages of the Pampean evolution at the western Gondwana margin in the Córdoba area (western Argentina). Sketches in A and B are modified from von Gosen and Prozzi (2010). In C, the situations during and after collision are summarized. The entire development is similar to that given by Schwartz et al. (2008). In our preliminary interpretation, the collision of the oceanic ridge was followed by the approach and collision of a continental terrane in the west, which is similar to the model of Siegesmund et al. (2010) (see text for further explanations).

and impacted pluton emplacement and continuing clastic sedimentation. However, evidence for these older relationships was not found during our field studies in the Sierra Norte or by the isotopic dates reported here.

Collision and D₂ Deformation (Early Cambrian)

The SIMS date of the granite porphyry (534 ± 5 Ma), intruded in the dextral mylonite zone south of San Pedro Norte (part of the “faja de

deformación Sauce Punco” of Martino et al., 1999a, 1999b) and locally affected by dextral mylonitization, provides an indication for the timing of this shearing, interpreted as the D₂ event (von Gosen and Prozzi, 2010). It shows that this stage of compressive deformation took place in the Early Cambrian just after cessation of the D₁ event (Fig. 16). This is supported by the SIMS date of the Talayaco granite mylonite (533 ± 4 Ma). It seems possible that the San Miguel gneiss, with its 533 ± 12 Ma SIMS age (Siegesmund et al., 2010), belongs to this stage, although the date is affected by a larger error.

The 531 ± 4 Ma SIMS date of the intrusion of the Agua del Río dacitic porphyry, affected by local dextral shearing at its eastern margin during cooling of the magmatic body, is interpreted as the age of crystallization. It points to the approximate timing of the latest stage of ductile dextral shearing, which was followed by uplift and subsequent intrusion of the high-level El Tío granite, dated at 530 ± 4 Ma (U-Pb, SIMS; Fig. 16). Our results fall in the 537 ± 4 Ma to 530 ± 4 Ma time span for dextral mylonitization constrained by U-Pb zircon (SIMS) dates in the southernmost part of the Sierra Norte (Iannizzotto et al., 2013). It should be noted that the younger age reported by Iannizzotto et al. (2013) from the postkinematic Villa Albertina granite is identical with the age of the El Tío granite given herein, suggesting a stage of uplift after dextral mylonitization also in the southernmost part of the Sierra Norte (see also following discussion).

Rapela et al. (1998a, 1998b) mentioned U-Pb zircon ages from granitoids of the Sierra Chica and Sierra Norte de Córdoba of 530 ± 3 Ma and suggested that the intrusion was partially coeval with, or closely followed, sedimentation of the Puncoviscana Formation (Rapela et al., 1998a). During our studies, however, we did not find field evidence for sedimentation during compressive D₂ deformation and intrusive activity in the Sierra Norte area.

Overall, the dates presented herein show that the D₂ deformation in the Sierra Norte area was also related to the Pampean orogeny in the Early Cambrian. This is according to the interpretations of Martino et al. (1999a, 1999b), Miró et al. (1999), and Rapela et al. (2007) for dextral shearing and mylonite formation of granites. In particular, our time estimates for dextral shearing and mylonitization confirm the interpretation of von Gosen and Prozzi (2010), who showed that the affected granitoids were synkinematically emplaced. The dates confirm the isotopic results and similar interpretation of Iannizzotto et al. (2013). An emplacement of the foliated granitoids in the Sierra Norte within shear zones, as proposed by Miró et al.

(1999), seems probable. It is possible that pluton emplacement was enabled in areas between right-stepping, en échelon and overlapping dextral strike-slip faults or shear zones, consistent with pluton emplacement in a transpressional setting (Iannizzotto et al., 2013).

The isotopic dates furthermore show that the Pampean D_2 event in the Sierra Norte area, recorded by dextral shearing and mylonitization, in time overlaps with the D_1 deformation. It seems that the D_2 event heterogeneously overprinted some areas of the Sierra Norte, while distinct parts remained unaffected. This part of the orogen, east of the accretionary prism in the Sierras de Córdoba and to the west (e.g., Northrup et al., 1998; Rapela et al., 1998a), was part of the upper (overriding) plate affected by a different style of compressive deformation in the Pampean history (von Gosen and Prozzi, 2010). Overall, both the initial D_1 deformation and the dextral mylonitization (D_2) seem to represent a continuous event that can be related to oblique (dextral) convergence between the overriding plate in the east and the subducting and finally colliding plate in the west (von Gosen and Prozzi, 2005a, 2010; Rapela et al., 2007; Iannizzotto et al., 2013). In their model, Iannizzotto et al. (2013) pointed to the possibility that deformation in the Pampean belt was diachronous and became progressively younger toward the north due to oblique dextral collision with a continental terrane. They suggested a large dextral displacement of the Pampean belt relative to the Río de la Plata craton during D_2 mylonitization. In our interpretation, ridge subduction (e.g., Schwartz et al., 2008) and collision might have been followed by collision of a continental terrane (Fig. 17C). This interpretation is similar to that proposed by Siegesmund et al. (2010).

Our time dates for the Pampean deformational and metamorphic events slightly contrast with the timing of the main events in the Sierras de Córdoba in the southwest, which took place at ca. 525 Ma and were followed by uplift and widespread anatexis at ca. 520 Ma (Rapela et al., 1998a). The deformational events in the Sierra Norte area, however, seem to coincide with the ca. 540 to ca. 520 Ma interval reported by Sims et al. (1998) for deformation and high-grade metamorphism during the Pampean orogeny. New SIMS U-Pb ages have shown, however, that the metamorphic history in the main ranges of the Sierras de Córdoba started at 553 Ma (Siegesmund et al., 2010).

Uplift and Postkinematic Magmatism (Early Cambrian)

Intrusive activity in the Sierra Norte is represented by granitoids emplaced during the D_2

deformation (synkinematic) and after cessation of the deformational history (postkinematic; von Gosen and Prozzi, 2010; Iannizzotto et al., 2013). The El Tío granite is a high-level postkinematic intrusion with chilled margins, abundant angular xenoliths of the deformed country rocks, and well-developed contact metamorphic aureole (von Gosen and Prozzi, 2010). These observations suggest that both Pampean deformational events were followed by an important phase of uplift. The 530 ± 4 Ma crystallization (SIMS) age of the undeformed El Tío granite indicates that D_1 and D_2 deformation ceased and uplift in the Sierra Norte area was ongoing in the Early Cambrian and continued through the Middle Cambrian (Fig. 16; see also following). The timing of this uplift event was regionally variable, since it occurred prior to intrusion and contact metamorphism at ca. 530 Ma in the Sierra Norte, whereas deformation and metamorphism in the Sierras de Córdoba continued up to ca. 520 Ma (Rapela et al., 1998a).

The SIMS zircon dates from the Rodeito rhyolite to dacite and El Escondido rhyolite (523 ± 5 Ma and 519 ± 4 Ma, respectively) also argue for uplift after cessation of Pampean deformation because neither rock shows ductile deformation. The younger ages in the Sierra Norte area seem to represent the final stage of the overall Pampean history. The slight deformation of the Ojo del Agua granite, with its 514 ± 4 Ma crystallization age (Stuart-Smith et al., 1999), may represent local late-stage Pampean deformation, deformation related to post-Pampean pluton emplacement, or a Famatinian (Ordovician) overprint. On the basis of the undeformed El Escondido rhyolite, however, it can be assumed that the Famatinian deformation did not affect the northern and northeastern areas of the Sierra Norte.

Continuing uplift in the Sierra Norte area was accompanied by the intrusion of the Los Burros dacite in the lowermost Middle Cambrian (512.6 ± 3.5 Ma, U-Pb, zircon, SIMS; Leal et al., 2003; Fig. 16). A roughly comparable age was found by Koukharsky et al. (2003) for a dacitic dike (514 ± 15 Ma, K-Ar, whole rock) cutting across the El Escondido granite, with its late Early Cambrian zircon SIMS date of 521 ± 4 Ma (see previous). The undeformed Ambargasta granite appears to belong to the final stage of the Pampean cycle as well, and on the basis of K-Ar biotite ages (Castellote, 1982), we assume a Middle Cambrian age. All the age data suggest that a combination of granitoid intrusions and rhyolitic to dacitic extrusions were emplaced after cessation of Pampean deformation in the Middle Cambrian.

Our results, combined with additional dates from Iannizzotto et al. (2013) and structural

observations of von Gosen and Prozzi (2010), demonstrate that many parts of the Sierra Norte–Ambargasta batholith consist of post- D_2 intrusions with different ages. The same is observed for extrusive units ranging from the Rodeito rhyolite to dacite at 523 ± 5 Ma (U-Pb, zircon, SIMS) to the Los Burros dacite at 512.6 ± 3.5 Ma (U-Pb, zircon, SIMS; Leal et al., 2003). An older U-Pb zircon age (TIMS) of 535 ± 8 Ma described by Miró et al. (2005) and Schwartz et al. (2008) from a porphyritic dacite in the area of the Los Burros dacite shows that the wide area of the Los Burros dacite does not consist of only lowermost Middle Cambrian magmatic rocks but also includes older components.

Intrusive igneous rocks with younger isotopic dates reported from the Sierra Norte de Córdoba (e.g., Rapela et al., 1991; Correa, 2003; present Fig. 16) and Sierras de Córdoba (e.g., Rapela et al., 1998a; Gromet and Simpson, 1999) are related to the Famatinian cycle and are interpreted as an effect of the Famatinian (Ordovician) subduction beneath the continental magmatic arc at the western margin of the Eastern Sierras Pampeanas unit.

CONCLUSIONS

New isotopic dates from the Sierra Norte de Córdoba, in combination with structural data and previously published isotopic dates and interpretations, suggest four successive stages of the sedimentary, magmatic, and tectonic evolution in the easternmost segment of the Eastern Sierras Pampeanas at the western pre-Andean Gondwana margin as follows.

(1) Deposition of the clastic sediments, which are interpreted as time equivalents of the Puncoviscana Formation (*sensu lato*), took place in the Ediacaran–Early Cambrian interval. Clastic sedimentation, accompanied by acid magmatism, is interpreted to be related to a passive-margin setting, probably on marginal west-Gondwanan crust (Fig. 17A).

(2) Sedimentation was directly followed by eastward-directed subduction beneath the west Gondwana margin and the generation of arc intrusions. In the developing upper plate (former passive margin), partitioned dextral transpressive D_1 deformation and regional metamorphism are assigned to a very short time interval during the Early Cambrian (Fig. 17B). An onset of subduction in the latest Neoproterozoic, however, cannot be excluded.

(3) Local D_2 deformation and metamorphism in the hanging-wall plate were accompanied by synkinematic intrusive activity. This stage of dextral shearing and mylonitization between ca. 534 and 531 Ma can be related to intraplate compression due to ridge subduction and/or

collision, which might have been followed by accretion of a continental terrane (Fig. 17C).

(4) Both short periods of Pampean (Early Cambrian) deformational events at the western pre-Andean Gondwana margin in the Sierra Norte de Córdoba were followed by uplift prior to 530 ± 4 Ma. Subsequent emplacement of different postkinematic intrusions and extrusive units suggests an end of the Pampean magmatic activity in the Middle Cambrian (Fig. 17C).

The undeformed igneous rocks in the Sierra Norte show that this segment of the easternmost Sierras Pampeanas was not significantly affected by Famatinian (Ordovician) deformation and metamorphism, which dominated along the western margin of the Eastern Sierras Pampeanas complex.

APPENDIX 1. SAMPLE PREPARATION

Samples were cleaned and crushed to a <10 mm grain size. Further pulverizing to a grain size of <1 mm was done by a disk mill. A heavy mineral separate from the sieved fraction of <0.25 mm was concentrated using a Wilfley-type wet shaking table. Further concentration of the zircons was achieved by heavy liquids and a Frantz isodynamic separator. The high-quality zircons for single-grain TIMS and SIMS analyses were selected from the bulk sample. Most of the zircons analyzed by TIMS were not air abraded; only the zircons marked in Table DR1 (sample CE-54D; see footnote 1) were abraded to ~90% of the original size.

APPENDIX 2. ANALYTICAL PROCEDURES (TIMS DATA)

The handpicked crystals were washed with 3.5 N HNO₃ for 30 min at 80 °C and then rinsed with distilled water and dried with acetone. Individual crystals and fractions were decomposed with 2 µl of 24 N HF in steel-cased multi- or single-hole Teflon containers for 3–4 days at 180 °C. The decomposed zircon was spiked with an appropriate amount (2 µl) of a ²⁰⁵Pb-²³⁵U tracer solution. After drying, the sample was converted to the chloride form with 2 µl of 6 N HCl overnight. The dried sample was loaded with a mixture of silica gel, HCl, and phosphoric acid on a Re single filament. Measurement of U and Pb was performed on a VG 354 mass spectrometer equipped with a Daly multiplier and an ion counting device by peak hopping, with Pb at 1250–1350 °C and U at 1400–1450 °C. Mass fractionation was controlled by the measurement of the standards NBS 982 (0.13%) and U 500 (0.06%). Samples with high concentrations of ²⁰⁵Tl were quickly heated to 1400 °C (within 10 min) and then kept at this temperature for a maximum of 2–3 min until the ²⁰⁵Tl signal fell to 1%–2% of the estimated spike intensity (given by the 205 signal). The worst measured ²⁰⁶Pb/²⁰⁴Pb ratio was 111 (for a sample dissolved in a new Teflon container); usually, the ratios were scattered around 500–1500, and the maximum measured ²⁰⁶Pb/²⁰⁴Pb ratio during the analyses was >5000, which is indicative of a constant and low procedural blank. Calculations were corrected with a maximum Pb blank of 0.01 pg with the following composition: 6/4 = 17.72, 7/4 = 15.52, 8/4 = 37.7, and a U blank of 0.5 pg. The initial Pb composition was calculated according to Stacey and Kramers' (1975) Pb evolution model.

Some of the performed analyses had to be rejected from concordia calculation due to their position above the concordia line. This effect appeared preferentially on zircons that had a high content of Tl. We presume that mainly an erroneous calculation of the Pb concentration led to the variable degree of discordance. The individually valid mass fractionation of Pb and U, according to the variable premeasurement conditions (in the course of getting rid of the Tl), could not be correctly verified by standard measurements at comparable conditions (flashing time and temperature).

The errors in the Table DR1 (see footnote 1) are quoted at the 1σ level, whereas the errors of the calculated discordias are given for the 95% confidence level. For data processing, programs were used as follows: PBDAT version 1.24, 30 July

1993, and ISOPLOT version 2.49 (2001) and 3.50, 21 June 2006, with kind permission of K. Ludwig (Berkeley Geochronology Center).

APPENDIX 3. ANALYTICAL PROCEDURES (SIMS DATA)

Zircons for SIMS analysis were handpicked under alcohol, mounted in a 2.5 cm epoxy round, and polished to expose the grain centers. The grains were imaged with transmitted light, reflected light, and CL prior to analysis. U-Pb isotopes and trace-element compositions were collected simultaneously on the sensitive high-resolution ion microprobe—reverse geometry (SHRIMP-RG) instrument at the U.S. Geological Survey—Stanford University Ion Probe Laboratory, Stanford, California, using a 25–30-µm-diameter spot size. The U-Pb analytical routine followed Barth and Wooden (2006), and data reduction utilized the SQUID program of Ludwig (2005). U-Pb isotopic composition was calibrated by replicate analyses of zircon standard R33 (419 Ma; Black et al., 2004), and U concentration was calibrated using zircon standard Madagascar Green (MAD, 4196 ppm U; Barth and Wooden, 2010). Calibration errors for ²⁰⁶Pb/²³⁸U ratios of R33 for the two analytical sessions were 0.62% and 0.39% (2σ). Ages were calculated as concordia ages or weighted mean ²⁰⁶Pb/²³⁸U ages using the Isoplot/Ex program of Ludwig (2003). Common Pb compositions were estimated from Stacey and Kramers (1975).

Trace-element data collection was simultaneous with U-Pb analysis, following Mazdab and Wooden (2006) and Mattinson et al. (2009). The REE routine measured ¹³⁹La, ¹⁴⁰Ce, ¹⁴⁶Nd, ¹⁴⁷Sm, ¹⁵³Eu, ¹⁵⁷Gd, ¹⁶³Dy, ¹⁶⁰Er, ¹⁶⁸Er, ¹⁷²Yb, ¹⁶⁰Er, and ¹⁸⁰Hf¹⁶O (Table 2). The routine for samples CE-66D and CE-54D included analysis of ¹⁷⁵Lu¹⁶O. Concentration calibrations used trace-element values of zircon standards CZ3 and MAD (Mazdab and Wooden, 2006). Estimated errors based on repeated analysis of CZ3 are 5%–10% for Y, Hf, Th, U, and the REEs except for La (30%) and include both analytical reproducibility and real abundance variation in the gem-quality zircon (cf. Mattinson et al., 2009). Chondrite-normalized REE plots (Fig. 8) use the chondrite REE abundances of Anders and Grevesse (1989) multiplied by a factor of 1.36 (Korotev, 1996). Chondrite-normalized values for Pr were calculated by interpolation ($Pr_{(N)} = La_{(N)}^{0.33} \times Nd_{(N)}^{0.67}$). Discussion of Eu anomalies is based on $Eu_{(N)}/Eu^*$ and $Ce_{(N)}/Ce^*$, with Eu^* and Ce^* calculated as geometric means (e.g., $Eu^* = [Sm_{(N)} \times Gd_{(N)}]^{0.5}$).

ACKNOWLEDGMENTS

Discussions with V.A. Ramos (Buenos Aires) helped to clarify the history of the Córdoba area. We are also grateful to L. DiNardo, J. Distas, D. Gregori (Bahía Blanca), and A.A. Bonalumi (Córdoba) for their support during field work. Many thanks go to J. Alvarez (Córdoba), G. Escorza (Puerto Madryn), and J.I. Falco (Bahía Blanca) for all their help during field work and many discussions. We thank the staff from the Central Laboratory for Geochronology at the University of Münster for support and use of the facilities, especially K. Mezger (now University of Bern) and T. Grund. We thank J. Wooden for help and discussion of trace-element and U-Pb data from the U.S. Geological Survey—Stanford University SHRIMP-RG (sensitive high-resolution ion microprobe—reverse geometry) laboratory. Many thanks go to K. Ludwig (Berkeley Geochronology Center) for permission to use his unpublished software ISOPLOT version 3.50 (21 June 2006). We are grateful to R.J. Pankhurst, S.O. Verdecchia, and an anonymous reviewer for constructive comments, suggestions, and corrections that helped improve the manuscript. This study was enabled by grants from the German Research Foundation (DFG) to W. von Gosen (projects Go 405/5–1 and 5–2), which are gratefully acknowledged.

REFERENCES CITED

Aceñolaza, F., and Aceñolaza, G., 2005, La Formación Puncoviciana y unidades estratigráficas vinculadas en el Neoproterozoico-Cámbrico temprano del noroeste Argentino: *Latin American Journal of Sedimentology and Basin Analysis*, v. 12, no. 2, p. 65–87.
 Aceñolaza, F.G., and Miller, H., 1982, Early Paleozoic orogeny in southern South America: *Precambrian Research*, v. 17, p. 133–146, doi:10.1016/0301-9268(82)90052-3.
 Aceñolaza, F.G., Miller, H., and Toselli, A.J., 1988, The Puncoviciana Formation (Late Precambrian–Early Cambrian)—

Sedimentology, tectonometamorphic history and age of the oldest rocks of NW Argentina, in Bahlburg, H., Breitzkreuz, C., and Giese, P., eds., *The Southern Central Andes: Contributions to Structure and Evolution of an Active Continental Margin*: Berlin, Springer, Lecture Notes in Earth Sciences, v. 17, p. 25–37.

- Aceñolaza, G.F., 2003, The Cambrian system in northwestern Argentina: Stratigraphical and palaeontological framework: *Geologica Acta*, v. 1, no. 1, p. 23–39.
 Adams, C.J., Miller, H., Toselli, A.J., and Griffin, W.L., 2008, The Puncoviciana Formation of northwest Argentina: U-Pb geochronology of detrital zircons and Rb-Sr metamorphic ages and their bearing on its stratigraphic age, sediment provenance and tectonic setting: *Neues Jahrbuch für Geologie und Paläontologie, Abhandlungen*, v. 247, no. 3, p. 341–352, doi:10.1127/0077-7749/2008/0247-0341.
 Adams, C.J., Miller, H., Aceñolaza, F.G., Toselli, A.J., and Griffin, W.L., 2011, The Pacific Gondwana margin in the late Neoproterozoic–early Paleozoic: Detrital zircon U-Pb ages from metasediments in northwest Argentina reveal their maximum age, provenance and tectonic setting: *Gondwana Research*, v. 19, p. 71–83, doi:10.1016/j.gr.2010.05.002.
 Anders, E., and Grevesse, N., 1989, Abundances of the elements: Meteoritic and solar: *Geochimica et Cosmochimica Acta*, v. 53, p. 197–214, doi:10.1016/0016-7037(89)90286-X.
 Astini, R.A., and Dávila, F.M., 2004, Ordovician back arc foreland and Ocolytic thrust belt development on the western Gondwana margin as a response to Pre-cordillera terrane accretion: *Tectonics*, v. 23, T4008, doi:10.1029/2003TC001620.
 Baldo, E.G., Demange, M., and Martino, R.D., 1996, Evolution of the Sierras de Córdoba, Argentina: Tectonophysics, v. 267, no. 1–4, p. 121–142, doi:10.1016/S0040-1951(96)00992-3.
 Baldo, E.G., Pankhurst, R.J., Rapela, C.W., Saavedra, J., and Mazieri, C., 1998, Granito “El Cerro,” magmatismo colisional famatiniano en el sector austral de la Sierra Norte–Ambargasta, Córdoba, in X Congreso Latinoamericano de Geología y VI Congreso Nacional de Geología Económica: Buenos Aires, Instituto de Geología y Recursos Minerales, Actas II, 374–378.
 Baldo, E.G., Saavedra, J., Rapela, C.W., Pankhurst, R.J., Casquet, C., and Galindo, C., 1999, Síntesis geocronológica de la evolución paleozoica inferior del borde sur occidental de Gondwana en las Sierras Pampeanas, Argentina, in *Busquets, P., Colombo, F., Pérez-Estaún, A., and Rodríguez Fernández, R., eds., Geología de los Andes Centrales Argentino-Chilenos: Acta Geológica Hispanica*, v. 32, no. 1–2, p. 17–28.
 Barth, A.P., and Wooden, J.L., 2006, Timing of magmatism following initial convergence at a passive margin, southwestern US Cordillera, and ages of lower crustal magma sources: *The Journal of Geology*, v. 114, p. 231–245, doi:10.1086/499573.
 Barth, A.P., and Wooden, J.L., 2010, Coupled elemental and isotopic analyses of polygenetic zircons from granitic rocks by ion microprobe, with implications for melt evolution and the source of granitic magmas: *Chemical Geology*, v. 277, p. 149–159, doi:10.1016/j.chemgeo.2010.07.017.
 Beder, R., 1922, Estudios geológicos en la Sierra de Córdoba especialmente de las calizas cristalino—granulosas y sus fenómenos de metamorfismo: Ministerio de Agricultura de la Nación, Dirección General de Minas, Geología y Hidrogeología, Boletín 33, Serie B (Geología), p. 1–86.
 Black, L.P., Kamo, S.L., Allen, C.M., Davis, D.W., Aleinikoff, J.N., Valley, J.W., Mundil, R., Campbell, I.H., Korsch, R.J., Williams, I.S., and Foudoulis, C., 2004, Improved ²⁰⁶Pb/²³⁸U microprobe geochronology by the monitoring of a trace-element-related matrix effect; SHRIMP, ID-TIMS, ELA-ICP-MS and oxygen isotope documentation for a series of zircon standards: *Chemical Geology*, v. 205, p. 115–140, doi:10.1016/j.chemgeo.2004.01.003.
 Bonalumi, A., and Baldo, E., 2002, Ordovician magmatism in the Sierras Pampeanas of Córdoba, in Aceñolaza, F.G., ed., *Aspects of the Ordovician System in Argentina: Tucumán, Argentina, INSUGEO, Serie Correlación Geológica*, v. 16, p. 243–256.

- Casquet, C., Rapela, C.W., Pankhurst, R.J., Baldo, E.G., Galindo, C., Fanning, C.M., Dahlquist, J.A., and Saavedra, J., 2012, A history of Proterozoic terranes in southern South America: From Rodinia to Gondwana: *Geoscience Frontiers*, v. 3, no. 2, p. 137–145, doi:10.1016/j.gsf.2011.11.004.
- Castellote, P.R., 1982, La Formación la Clemira y edad de su metamorfismo (Sierra de Ambargasta, Provincia de Santiago del Estero): *Acta Geológica Lilloana*, v. 16, no. 1, p. 71–76.
- Castellote, P.R., 1985a, Algunas observaciones geológicas en las Sierras de Ambargasta y Sumampa (Provincia de Santiago del Estero): *Acta Geológica Lilloana*, v. 16, no. 2, p. 259–269.
- Castellote, P.R., 1985b, La Formación "Poza del Macho," integrante del basamento metamórfico de la Sierra de Ambargasta, Provincia de Santiago del Estero: *Acta Geológica Lilloana*, v. 16, no. 2, p. 275–280.
- Cordani, U.G., Pimentel, M.M., Ganade de Araújo, C.E., Basei, M.A.S., Fuck, R.A., and Girardi, V.A.V., 2013, Was there an Ediacaran Clymene Ocean in central South America?: *American Journal of Science*, v. 313, p. 517–539, doi:10.2475/06.2013.01.
- Correa, M.J., 2003, Petrología y edad K/Ar de diques relacionados a la Formación Oncán, Sierra de Ambargasta, Santiago del Estero: *Revista de la Asociación Geológica Argentina*, v. 58, no. 4, p. 664–668.
- Dahlquist, J.A., Pankhurst, R.J., Rapela, C.W., Galindo, C., Alasino, P., Fanning, C.M., Saavedra, J., and Baldo, E., 2008, New SHRIMP U-Pb data from the Famatina complex: Constraining Early–mid-Ordovician Famatian magmatism in the Sierras Pampeanas, Argentina: *Geologica Acta*, v. 6, no. 4, p. 319–333.
- Dahlquist, J.A., Pankhurst, R.J., Gaschnig, R.M., Rapela, C.W., Casquet, C., Alasino, P.H., Galindo, C., and Baldo, E.G., 2013, Hf and Nd isotopes in Early Ordovician to early Carboniferous granites as monitors of crustal growth in the proto-Andean margin of Gondwana: *Gondwana Research*, v. 23, p. 1617–1630, doi:10.1016/j.gr.2012.08.013.
- de los Hoyos, C.R., Willner, A.P., Larrovere, M.A., Rossi, J.N., Toselli, A.J., and Basei, M.A.S., 2011, Tectonothermal evolution and exhumation history of the Paleozoic proto-Andean Gondwana margin crust: The Famatian belt in NW Argentina: *Gondwana Research*, v. 20, p. 309–324, doi:10.1016/j.gr.2010.12.004.
- Ducea, M.N., Otamendi, J.E., Bergantz, G., Stair, K.M., Valencia, V.A., and Gehrels, G.E., 2010, Timing constraints on building an intermediate plutonic arc crustal section: U-Pb zircon geochronology of the Sierra Valle Fértil-La Huerta, Famatinian arc, Argentina: *Tectonics*, v. 29, no. 4, doi:10.1029/2009TC002615.
- Escayola, M.P., van Staal, C.R., and Davis, W.J., 2011, The age and tectonic setting of the Puncovicana Formation in northwestern Argentina: An accretionary complex related to Early Cambrian closure of the Puncovicana Ocean and accretion of the Arequipa-Antofalla block: *Journal of South American Earth Sciences*, v. 32, p. 438–459, doi:10.1016/j.jsames.2011.04.013.
- González, P.D., Sato, A.M., Llambías, E.J., Basei, M.A.S., and Vlach, S.R.F., 2004, Early Paleozoic structural and metamorphic evolution of western Sierra de San Luis (Argentina), in relation to Cuyania accretion: *Gondwana Research*, v. 7, no. 4, p. 1157–1170, doi:10.1016/S1342-937X(05)71091-1.
- Gromet, L.P., and Simpson, C., 1999, Age of the Paso del Carmen pluton and implications for the duration of the Pampean orogeny, Sierras de Córdoba, in XIV Congreso Geológico Argentino (Salta): Buenos Aires, Asociación Geológica Argentina, Actas, v. I, p. 149–151.
- Gromet, L.P., Otamendi, J.E., Miró, R.C., Demichelis, A.H., Schwartz, J.J., and Tibaldi, A.M., 2005, The Pampean orogeny: Ridge subduction or continental collision?, in Pankhurst, R.J., and Veiga, G.D., eds., *Gondwana 12: Geological and Biological Heritage of Gondwana*, Abstracts: Córdoba, Argentina, Academia Nacional de Ciencias, p. 185–186.
- Guerreschi, A.B., and Martino, R.D., 2002, Evolución textural de las corneanas de La Clemira, Sierra de Ambargasta, Santiago del Estero, Argentina, in Cingolani, C.A., Cabaleri, N., Linares, E., López de Luchi, M.G., Osters, H.A., and Panarello, H.O., eds., XV Congreso Geológico Argentino (El Calafate): Buenos Aires, Asociación Geológica Argentina, Actas, v. II, p. 180–183.
- Iannizzotto, N.F., Rapela, C.W., and Baldo, E.G.A., 2011, Nuevos datos geocronológicos, geoquímicos e isotópicos del Batolito de Sierra Norte–Ambargasta en su sector más austral, Provincia de Córdoba, in Leanza, H., Franchini, M., Impiccini, A., Pettinari, G., Sigismondi, M., Pons, J., and Tunik, M., eds., XVIII Congreso Geológico Argentino (Neuquén): Neuquén, Argentina, Asociación Geológica Argentina, Actas (CD), p. 190–191.
- Iannizzotto, N.F., Rapela, C.W., Baldo, E.G.A., Galindo, C., Fanning, C.M., and Pankhurst, R.J., 2013, The Sierra Norte–Ambargasta batholith: Late Ediacaran–Early Cambrian magmatism associated with Pampean transpressional tectonics: *Journal of South American Earth Sciences*, v. 42, p. 127–143, doi:10.1016/j.jsames.2012.07.009.
- Keppie, J.D., and Bahlburg, H., 1999, Puncovicana Formation of northwestern and central Argentina: Passive margin or foreland basin deposit?, in Ramos, V.A., and Keppie, J.D., eds., *Laurentia-Gondwana Connections before Pangea*: Geological Society of America Special Paper 336, p. 139–143.
- Korotev, R.L., 1996, A self-consistent compilation of elemental concentration data for 93 geochemical reference samples: *Geostandards Newsletter*, v. 20, p. 217–245, doi:10.1111/j.1751-908X.1996.tb00185.x.
- Koukharsky, M., Munizaga, F., Leal, P., Correa, M.J., and de Brodtkorb, M.K., 1999, New K/Ar ages in the Ambargasta and Norte de Córdoba ranges, Argentina, in II Latin American Symposium on Isotope Geology (Villa Carlos Paz/Córdoba): Villa Carlos Paz/Córdoba, Servicio Geológico Minero Argentino, Actas, p. 76–77.
- Koukharsky, M., de Brodtkorb, M.K., Kay, S.M., and Munizaga, F., 2003, La Formación Balbuena, integrante del arco magmático pampeano en la Sierra de Ambargasta, provincia de Santiago del Estero: *Revista de la Asociación Geológica Argentina*, v. 58, no. 4, p. 583–592.
- Kraemer, P.E., Escayola, M.P., and Martino, R.D., 1995, Hipótesis sobre la evolución tectónica neoproterozoica de las Sierras Pampeanas de Córdoba (30°40'–32°40'), Argentina: *Revista de la Asociación Geológica Argentina*, v. 50, no. 1–4, p. 47–59.
- Larrovere, M.A., de los Hoyos, C.R., Toselli, A.J., Rossi, J.N., Basei, M.A.S., and Belmar, M.E., 2011, High T/P evolution and metamorphic ages of the migmatitic basement of northern Sierras Pampeanas, Argentina: Characterization of a mid-crustal segment of the Famatinian belt: *Journal of South American Earth Sciences*, v. 31, p. 279–297, doi:10.1016/j.jsames.2010.11.006.
- Leal, P.R., Hartmann, L.A., Santos, J.O.S., Miró, R.C., and Ramos, V.A., 2003, Volcanismo postorogénico en el extremo norte de las Sierras Pampeanas Orientales: Nuevos datos geocronológicos y sus implicancias tectónicas: *Revista de la Asociación Geológica Argentina*, v. 58, no. 4, p. 593–607.
- Lira, R., Millone, H.A., Kirschbaum, A.M., and Moreno, R.S., 1997, Calc-alkaline arc granitoid activity in the Sierra Norte–Ambargasta ranges, central Argentina: *Journal of South American Earth Sciences*, v. 10, no. 2, p. 157–177, doi:10.1016/S0895-9811(97)00013-8.
- Llambías, E.J., Gregori, D., Basei, M.A., Varela, R., and Prozzi, C., 2003, Ignimbritas riolíticas neoproterozoicas en la Sierra Norte de Córdoba: ¿Evidencia de un arco magmático temprano en el ciclo Pampeano?: *Revista de la Asociación Geológica Argentina*, v. 58, no. 4, p. 572–582.
- Lucero, H.N., 1958, Sobre las psamitas y conglomerados arcóscicos intercalados en el basamento de las Sierras de Córdoba: *Comunicaciones del Museo de Mineralogía y Geología, Universidad Nacional de Córdoba*, v. 34, p. 1–23.
- Lucero, H.N., 1969, Descripción geológica de las Hojas 16 h, Poza Grande y 17 h, Chuña Huasi, Provincias de Córdoba y Santiago del Estero: *Carta Geológico-Económica de la República Argentina, escala 1:200,000*: Buenos Aires, Ministerio de Economía y Trabajo, Dirección Nacional de Geología y Minería Boletín 107, p. 1–28.
- Lucero Michaut, H.N., 1979, Sierras Pampeanas del norte de Córdoba, sur de Santiago del Estero, borde oriental de Catamarca y ángulo sudeste de Tucumán, in Turner, J.C.M., ed., Segundo Simposio de Geología Regional Argentina: Argentina, Academia Nacional de Ciencias Córdoba, v. I, p. 293–347. Córdoba,
- Lucero Michaut, H.N., 1981, Contribución al conocimiento geológico del cordón oriental de la Sierra Norte entre Simbolar y el límite con Santiago del Estero: *Boletín de la Asociación Geológica de Córdoba*, v. 4, no. 1–4, p. 223–235.
- Lucero Michaut, H.N., and Daziano, C.O., 1985, Sobre la presencia de rocas pertenecientes a la Formación "La Lidia-Simbolhuasi" en el bajo faldeo occidental de la Sierra de Sauce Puncu (Sierra Norte de Córdoba): *Boletín de la Asociación Geológica de Córdoba*, v. 7, p. 411–415.
- Lucero Michaut, H.N., and Daziano, C.O., 1988, Información preliminar sobre el estudio de la Formación "La Lidia-Simbolhuasi" (entre las quebradas de Talayaco y La Hoyada), Sauce Puncu–Sierra Norte de Córdoba: *Boletín de la Asociación Geológica de Córdoba*, v. 9, p. 560–570.
- Ludwig, K.R., 1993, PBDAT: A Computer Program for Processing Pb-U-Th Isotope Data: U.S. Geological Survey Open-File Report, 88–542, 33 p.
- Ludwig, K.R., 2001, Isoplot/Ex, Rev. 2.49. A Geochronological Toolkit for Microsoft Excel: Berkeley Geochronology Center Special Publication 1a.
- Ludwig, K.R., 2003, User's Manual for Isoplot 3.00: A Geochronological Toolkit for Microsoft Excel: Berkeley Geochronology Center Special Publication 1, 40 p.
- Ludwig, K.R., 2005, Squid Version 1.13b: A User's Manual: Berkeley Geochronology Center Special Publication 2, p. 1–22.
- Ludwig, K., 2006, ISOPLOT Version 3.50 (June 21, 2006): A Plotting and Regression Program for Radiogenic Isotope Data: Berkeley, California, Berkeley Geochronology Center.
- Martino, R.D., 2003, La fajas de deformación dúctil en las Sierras Pampeanas de Córdoba: Una reseña general: *Revista de la Asociación Geológica Argentina*, v. 58, no. 4, p. 549–571.
- Martino, R.D., 2004, Análisis estructural de deformaciones sinsedimentarias: Los pliegues de la Formación El Escondido, Sierra de Ambargasta, Santiago del Estero, in Martino, R., and Guerreschi, A., eds., *Avances in Microtectónica y Geología Estructural: Asociación Geológica Argentina, Serie D, Publicación Especial 7*, p. 20–26.
- Martino, R.D., and Guerreschi, A.B., 2004, Estructura de las metamorfitas de Poza del Macho, Sierra de Ambargasta, Santiago del Estero, in Martino, R., and Guerreschi, A., eds., *Avances in Microtectónica y Geología Estructural: Asociación Geológica Argentina, Serie D, Publicación Especial 7*, p. 131–136.
- Martino, R.D., and Guerreschi, A.B., 2005, Estructuras primarias, secundarias y evolución estructural de las corneanas de La Clemira, Sierra de Ambargasta, Santiago del Estero: *Revista de la Asociación Geológica Argentina*, v. 60, no. 2, p. 327–335.
- Martino, R., Pinceyra, R., Guerreschi, A., and Sfragulla, J., 1999a, Transcurrencia paralela al arco magmático de la Sierra Norte de Córdoba: La faja de deformación Sauce Puncu, in XIV Congreso Geológico Argentino (Salta): Buenos Aires, Asociación Geológica Argentina, Actas, v. I, p. 37–38.
- Martino, R., Pinceyra, R., Guerreschi, A., and Sfragulla, J., 1999b, La faja de deformación Sauce Puncu, Sierra Norte, Córdoba, Argentina: *Revista de la Asociación Geológica Argentina*, v. 53, no. 4, p. 436–440.
- Martino, R.D., Collo, G., and Pinceyra, R.A., 2004, Las metamorfitas de bajo grado del oeste de San Francisco del Chañar: Caracterización petrográfica y estructura interna, Sierra Norte de Córdoba, in Martino, R., and Guerreschi, A., eds., *Avances in Microtectónica y Geología Estructural: Asociación Geológica Argentina, Serie D, Publicación Especial 7*, p. 76–81.
- Massabie, A., Mutti, D., and Nestiero, O., 2002, Edad, afinidades geoquímicas y tectónicas del pórfido riolítico de La Lidia, Sierra Norte de Córdoba: *Revista de la Asociación Geológica Argentina*, v. 57, no. 1, p. 80–84.
- Mattinson, C.G., Wooden, J.L., Zhang, J.X., and Bird, D.K., 2009, Paragneiss zircon geochronology and trace element geochemistry, North Qaidam HP/UHP terrane, western China: *Journal of Asian Earth Sciences*, v. 35, p. 298–309, doi:10.1016/j.jseas.2008.12.007.
- Mattinson, J.M., 2005, Zircon U-Pb chemical abrasion ("CA-TIMS") method: Combined annealing and multi-step partial dissolution analysis for improved precision and

- accuracy of zircon ages: *Chemical Geology*, v. 220, p. 47–66, doi:10.1016/j.chemgeo.2005.03.011.
- Mazdab, F.M., and Wooden, J.L., 2006, Trace element analysis in zircon by ion microprobe (SHRIMP-RG): technique and applications: *Geochimica et Cosmochimica Acta*, v. 70, p. A405, doi:10.1016/j.gca.2006.06.817.
- Methol, E.J., 1958, Descripción Geológica de la Hoja 18 I, Deán Funes. Tulumba (Córdoba). Carta Geológico-Económica de la República Argentina Escala 1:200,000: Buenos Aires, Ministerio de Economía de la Nación, Dirección Nacional de Geología y Minería Boletín 88, p. 1–69.
- Millone, H.A., Tassinari, C.C.G., Lira, R., and Poklepovic, M.F., 2003, Age and strontium-neodymium isotope geochemistry of granitoids of the Sierra Norte-Ambar-gasta batholith, central Argentina, in *IV South American Symposium on Isotope Geology, Short Papers, August 24–27, 2003: Salvador de Bahía, Brazil, Companhia Baina de Pesquisa Mineral, Institut de recherche pour le development*, p. 617–620.
- Miró, R., and Sapp, M., 2000, Carta Geológica Villa Ojo de Agua, 2963-III, Provincias de Santiago del Estero y Córdoba, Escala 1:250,000: Buenos Aires, Argentina, SEGEMAR, Instituto de Geología y Recursos Minerales.
- Miró, R.C., Gaido, M.F., and Candiani, J.C., 1999, Fajas de deformación del batolito Sierra Norte de Córdoba y Santiago del Estero, in *XIV Congreso Geológico Argentino (Salta): Buenos Aires, Asociación Geológica Argentina, Actas*, v. I, p. 152–155.
- Miró, R.C., Schwartz, J., and Gromet, P., 2005, Magmatismo calcoalcalino en la Sierra Norte de Córdoba. Su extensión temporal, in Aceñolaza, F.G., Aceñolaza, G.F., Hünicken, M., Rossi, J.N., and Toselli, A.J., eds., *Simpósio Bodenbender: Tucumán, Argentina, INSUGEO, Serie Correlación Geológica*, v. 19, p. 199–210.
- Northrup, C.J., Simpson, C., and Gromet, P.L., 1998, Early Paleozoic history of the Eastern Sierras Pampeanas, Argentina: Development of a Cambrian arc and accretionary prism along the margin of Gondwana, in *X Congreso Latinoamericano de Geología y VI Congreso Nacional de Geología Económica (Buenos Aires): Buenos Aires, Instituto de Geología y Recursos Minerales, Actas*, v. II, p. 400–403.
- Pankhurst, R., Rapela, C.W., Saavedra, J., Baldo, E., Dahlquist, J., Pascua, I., and Fanning, C.M., 1998, The Famatinian magmatic arc in the central Sierras Pampeanas: An Early to mid-Ordovician continental arc on the Gondwana margin, in Pankhurst, R.J., and Rapela, C.W., eds., *The Proto-Andean Margin of Gondwana: Geological Society of London Special Publication 142*, p. 343–367.
- Pankhurst, R., Rapela, C., and Fanning, C.M., 2000, Age and origin of coeval TTG, I- and S-type granites in the Famatinian belt of NW Argentina: *Transactions of the Royal Society of Edinburgh—Earth Sciences*, v. 91, p. 151–168, doi:10.1017/S0263593300007343.
- Piñán-Llamas, A., and Simpson, C., 2006, Deformation of Gondwana margin turbidites during the Pampean orogeny, north-central Argentina: *Geological Society of America Bulletin*, v. 118, no. 9–10, p. 1270–1279, doi:10.1130/B25915.1.
- Prozzi, C.R., 1990, Consideraciones acerca del basamento de San Luis, Argentina, in *XI Congreso Geológico Argentino (San Juan): Buenos Aires, Asociación Geológica Argentina, Actas*, v. I, p. 452–455.
- Prozzi, C., and Ramos, G., 1988, La Formación San Luis: Primeras Jornadas de Trabajo de Sierras Pampeanas (San Luis, 24 al 26 de Agosto), abstract, p. 1.
- Quartino, B.J., Massabie, A.C., and Morelli, J.R., 1978, Formaciones eopaleozoicas en el norte de Córdoba y sur de Santiago del Estero, su magmatismo y significado geológico: *Revista de la Asociación Geológica Argentina*, v. 33, no. 1, p. 90–92.
- Ramos, V.A., 1988, Late Proterozoic–early Paleozoic of South America—A collisional history: *Episodes*, v. 11, no. 3, p. 168–174.
- Ramos, V.A., 1999, Rasgos estructurales del territorio argentino. 1. Evolución tectónica de la Argentina, in *Caminos, R., ed., Geología Argentina: Instituto de Geología y Recursos Minerales, Anales*, v. 29, capítulo 24, p. 715–759.
- Ramos, V.A., 2004, Cuyania, an exotic block to Gondwana: Review of a historical success and the present problems: *Gondwana Research*, v. 7, no. 4, p. 1009–1026, doi:10.1016/S1342-937X(05)71081-9.
- Ramos, V.A., Vujovich, G., Martino, R., and Otamendi, J., 2010, Pampia: A large cratonic block missing in the Rodinia supercontinent: *Journal of Geodynamics*, v. 50, no. 3–4, p. 243–255, doi:10.1016/j.jog.2010.01.019.
- Rapela, C.W., Pankhurst, R.J., and Bonalumi, A.A., 1991, Edad y geoquímica del pórfido granítico de Oncán, Sierra Norte de Córdoba, Sierras Pampeanas, Argentina, in *VI Congreso Geológico Chileno: Santiago, Servicio Nacional de Geología y Minería, Chile, Resúmenes Ampliados*, p. 19–22.
- Rapela, C.W., Pankhurst, R.J., Casquet, C., Baldo, E., Saavedra, J., Galindo, C., and Fanning, C.M., 1998a, The Pampean orogeny of the southern proto-Andes: Cambrian continental collision in the Sierras de Córdoba, in Pankhurst, R.J., and Rapela, C.W., eds., *The Proto-Andean Margin of Gondwana: Geological Society of London Special Publication 142*, p. 181–217.
- Rapela, C.W., Pankhurst, R.J., Casquet, C., Baldo, E.G., Saavedra, J., and Galindo, C., 1998b, Las colisiones continentales pampeana y famatiniana, in *X Congreso Latinoamericano de Geología y VI Congreso Nacional de Geología Económica (Buenos Aires): Buenos Aires, Instituto de Geología y Recursos Minerales, Actas*, v. II, p. 404.
- Rapela, C.W., Pankhurst, R.J., Casquet, C., Baldo, E., Saavedra, J., and Galindo, C., 1998c, Early evolution of the Proto-Andean margin of South America: *Geology*, v. 26, no. 8, p. 707–710, doi:10.1130/0091-7613(1998)026<0707:EOT PA>2.3.CO;2.
- Rapela, C.W., Casquet, C., Baldo, E., Dahlquist, J., Pankhurst, R.J., Galindo, C., and Saavedra, J., 2001, Las orogénesis del Paleozoico Inferior en el margen proto-andino de América del Sur, Sierras Pampeanas, Argentina: *Journal of Iberian Geology*, v. 27, p. 23–41.
- Rapela, C.W., Fanning, C.M., and Pankhurst, R.J., 2005, The Rio de La Plata craton: The search for its full extent, in Pankhurst, R.J., and Veiga, G.D., eds., *Gondwana 12: Geological and Biological Heritage of Gondwana (Mendoza)*, Abstracts: Córdoba, Argentina, Academia Nacional de Ciencias, p. 308.
- Rapela, C.W., Pankhurst, R.J., Casquet, C., Fanning, C.M., Baldo, E.G., González-Casado, J.M., Galindo, C., and Dahlquist, J., 2007, The Rio de la Plata craton and the assembly of SW Gondwana: *Earth-Science Reviews*, v. 83, no. 1–2, p. 49–82, doi:10.1016/j.earscirev.2007.03.004.
- Rapela, C.W., Fanning, C.M., Casquet, C., Pankhurst, R.J., Spalletti, L., Poiré, D., and Baldo, E.G., 2011, The Rio de la Plata craton and the adjoining Pan-African/Brasiliano terranes: Their origins and incorporation into southwestern Gondwana: *Gondwana Research*, v. 20, p. 673–690, doi:10.1016/j.gr.2011.05.001.
- Sato, A.M., González, P.D., and Llambías, E.J., 2003, Evolución del orógeno Famatiniano en la Sierra de San Luis: Magmatismo de arco, deformación y metamorfismo de bajo a alto grado: *Revista de la Asociación Geológica Argentina*, v. 58, no. 4, p. 487–504.
- Schwartz, J.J., and Gromet, L.P., 2004, Provenance of a late Proterozoic–Early Cambrian basin, Sierras de Córdoba, Argentina: *Precambrian Research*, v. 129, no. 1–2, p. 1–21, doi:10.1016/j.precamres.2003.08.011.
- Schwartz, J.J., Gromet, L.P., and Miró, R., 2008, Timing and duration of the calc-alkaline arc of the Pampean orogeny: Implications for the late Neoproterozoic to Cambrian evolution of western Gondwana: *The Journal of Geology*, v. 116, p. 39–61, doi:10.1086/524122.
- Siegesmund, S., Steenken, A., Martino, R.D., Wemmer, K., López de Luchi, M.G., Frei, R., Presnyakov, S., and Guerreschi, A., 2010, Time constraints on the tectonic evolution of the Eastern Sierras Pampeanas (central Argentina): *International Journal of Earth Sciences (Geologische Rundschau)*, v. 99, p. 1199–1226, doi:10.1007/s00531-009-0471-z.
- Simpson, C., Law, R.D., Gromet, P.L., Miró, R., and Northrup, C.J., 2003, Paleozoic deformation in the Sierras de Córdoba and Sierra de las Minas, eastern Sierras Pampeanas, Argentina: *Journal of South American Earth Sciences*, v. 15, p. 749–764, doi:10.1016/S0895-9811(02)00130-X.
- Sims, J.P., Ireland, T.R., Camacho, A., Lyons, P., Pieters, P.E., Skirrow, R.G., Stuart-Smith, P.G., and Miró, R., 1998, U-Pb, Th-Pb and Ar-Ar geochronology from the southern Sierras Pampeanas, Argentina: Implications for the Paleozoic tectonic evolution of the western Gondwana margin, in Pankhurst, R.J., and Rapela, C.W., eds., *The Proto-Andean Margin of Gondwana: Geological Society of London Special Publication 142*, p. 259–281.
- Söllner, F., de Brodtkorb, M.K., Miller, H., Pezzutti, N.E., and Fernández, R.R., 2000, U-Pb zircon ages of metavolcanic rocks from the Sierra de San Luis, Argentina: *Revista de la Asociación Geológica Argentina*, v. 55, no. 1–2, p. 15–22.
- Stacey, J.S., and Kramers, J.D., 1975, Approximation of terrestrial lead evolution by a two-stage model: *Earth and Planetary Science Letters*, v. 26, p. 207–221, doi:10.1016/0012-821X(75)90088-6.
- Steenken, A., Siegesmund, S., López de Luchi, M.G., Frei, R., and Wemmer, K., 2006, Neoproterozoic to early Paleozoic events in the Sierra de San Luis: Implications for the Famatinian geodynamics in the Eastern Sierras Pampeanas (Argentina): *Journal of the Geological Society of London*, v. 163, no. 6, p. 965–982, doi:10.1144/0016-76492005-064.
- Steenken, A., López de Luchi, M.G., Martínez Dopico, C., Drobe, M., Wemmer, K., and Siegesmund, S., 2011, The Neoproterozoic–early Paleozoic metamorphic and magmatic evolution of the Eastern Sierras Pampeanas: An overview: *International Journal of Earth Sciences (Geologische Rundschau)*, v. 100, no. 2–3, p. 465–488, doi:10.1007/s00531-010-0624-0.
- Stuart-Smith, P.G., Camacho, A., Sims, J.P., Skirrow, R.G., Lyons, P., Pieters, P.E., Black, L.P., and Miró, R., 1999, Uranium-lead dating of felsic magmatic cycles in the southern Sierras Pampeanas, Argentina: Implications for the tectonic development of the proto-Andean Gondwana margin, in Ramos, V.A., and Keppie, J.D., eds., *Laurentia-Gondwana Connections before Pangea: Geological Society of America Special Paper 336*, p. 87–114.
- Thomas, W.A., and Astini, R.A., 2003, Ordovician accretion of the Argentine Precordillera terrane to Gondwana: A review: *Journal of South American Earth Sciences*, v. 16, no. 1, p. 67–79, doi:10.1016/S0895-9811(03)00019-1.
- Toselli, A.J., Aceñolaza, G.F., Miller, H., Adams, C., Aceñolaza, F.G., and Rossi, J.N., 2012, Basin evolution of the margin of Gondwana at the Neoproterozoic/Cambrian transition: The Puncoviscana Formation of northwest Argentina: *Neues Jahrbuch für Geologie und Paläontologie, Abhandlungen*, v. 265, no. 1, p. 70–95.
- Verdecchia, S.O., Baldo, E.G., Benedetto, J.L., and Borghi, P.A., 2007, The first shelly fauna from metamorphic rocks of the Sierras Pampeanas (La Cébila Formation, Sierra de Ambato, Argentina): Age and paleogeographic implications: *Ameghiniana*, v. 44, no. 2, p. 493–498.
- Verdecchia, S.O., Casquet, C., Baldo, E.G., Pankhurst, R.J., Rapela, C.W., Fanning, M., and Galindo, C., 2011, Mid- to Late Cambrian docking of the Rio de la Plata craton to southwestern Gondwana: Age constraints from U-Pb SHRIMP detrital zircon ages from Sierras de Ambato and Velasco (Sierras Pampeanas, Argentina): *Journal of the Geological Society of London*, v. 168, no. 4, p. 1061–1071, doi:10.1144/0016-76492010-143.
- von Gosen, W., and Prozzi, C., 1998, Structural evolution of the Sierra de San Luis (Eastern Sierras Pampeanas, Argentina): Implications for the proto-Andean margin of Gondwana, in Pankhurst, R.J., and Rapela, C.W., eds., *The Proto-Andean Margin of Gondwana: Geological Society of London Special Publication 142*, p. 235–258.
- von Gosen, W., and Prozzi, C., 2005a, Clastic metasediments in the Sierras Norte de Córdoba (Argentina): Pampean compression and magmatism, Llambías, E., de Barrio, R., González, P., and Leal, P., eds., *XVI Congreso Geológico Argentino (La Plata): La Plata, Asociación Geológica Argentina, Actas*, v. I, p. 247–248.
- von Gosen, W., and Prozzi, C., 2005b, Clastic metasediments in the Sierras Norte de Córdoba (Argentina): Stages of sedimentation, magmatism and initial tectonics, in Llambías, E., de Barrio, R., González, P., and Leal, P., eds., *XVI Congreso Geológico Argentino (La Plata): La Plata, Asociación Geológica Argentina, Actas*, v. I, p. 249–250.
- von Gosen, W., and Prozzi, C., 2005c, Deformation of an early Paleozoic magmatic arc related to terrane collision: The Sierra de San Luis (Eastern Sierras Pampeanas,

- Argentina): Neues Jahrbuch für Geologie und Paläontologie, Abhandlungen, v. 238, no. 1, p. 107–160 (www.schweizerbart.de).
- von Gosen, W., and Prozzi, C., 2005d, Late Proterozoic to Cambrian evolution in the Sierras Norte de Córdoba (Argentina): Implications for the pre-Andean Gondwana margin, in Pankhurst, R.J., and Veiga, G.D., eds., *Gondwana 12: Geological and Biological Heritage of Gondwana*, Abstracts: Córdoba, Argentina, Academia Nacional de Ciencias, p. 371.
- von Gosen, W., and Prozzi, C., 2009, Late Proterozoic to Early Cambrian sedimentation and magmatism at the western Gondwana margin: Metasedimentary rocks in the Sierras Norte de Córdoba (Argentina): Neues Jahrbuch für Geologie und Paläontologie, Abhandlungen, v. 253, no. 1, p. 79–101, www.schweizerbart.de, doi:10.1127/0077-7749/2009/0253-0079.
- von Gosen, W., and Prozzi, C., 2010, Pampean deformation in the Sierra Norte de Córdoba, Argentina: Implications for the collisional history at the western pre-Andean Gondwana margin: *Tectonics*, v. 29, TC2012, doi:10.1029/2009TC002580.
- von Gosen, W., Loske, W., and Prozzi, C., 2002, New isotopic dating of intrusive rocks in the Sierra de San Luis (Argentina): Implications for the geodynamic history of the Eastern Sierras Pampeanas: *Journal of South American Earth Sciences*, v. 15, p. 237–250, doi:10.1016/S0895-9811(02)00016-0.
- von Gosen, W., Martínez, J.C., Prozzi, C., and Loske, W., 2005, The El Escondido Formation (Santiago del Estero Province, Argentina): Sedimentation, deformation, and age, in Llambías, E., de Barrio, R., González, P., and Leal, P., eds. *XVI Congreso Geológico Argentino (La Plata): La Plata, Asociación Geológica Argentina, Actas*, v. 1, p. 257–258.
- von Gosen, W., Buggisch, W., and Prozzi, C., 2009, Provenance and geotectonic setting of Late Proterozoic–Early Cambrian metasediments in the Sierras de Córdoba and Guasayán (western Argentina): A geochemical approach: Neues Jahrbuch für Geologie und Paläontologie, Abhandlungen, v. 251, no. 3, p. 257–284, www.schweizerbart.de, doi:10.1127/0077-7749/2009/0251-0257.
- Walker, J.D., Geissman, J.W., Bowring, S.A., and Babcock, L.E., compilers, 2012, *Geological Society of America Geologic Time Scale*, v. 4.0: Boulder, Colorado, Geological Society of America.
- Whitmeyer, S.J., and Simpson, C., 2004, Regional deformation of the Sierra de San Luis, Argentina: Implications for the Paleozoic development of western Gondwana: *Tectonics*, v. 23, TC1005, doi:10.1029/2003TC001542.
- Williams, I.S., 1998, U-Pb by ion microprobe, in McKibben, M.A., Shanks, W.C., and Ridley, W.I., eds., *Applications of Microanalytical Techniques to Understanding Mineralizing Processes: Society of Economic Geologists, Reviews in Economic Geology*, v. 7, p. 1–35.
- Willner, A.P., 1990, Division tectonometamorfica del basamento del Noroeste Argentino, in Aceñolaza, F., Miller, H., and Toselli, A.J., eds., *El Ciclo Pampeano en el Noroeste Argentino: Tucumán, Argentina, INSUGEO, Serie Correlación Geológica*, v. 4, p. 113–159.
- Willner, A.P., and Miller, H., 1986, Structural division and evolution of the Lower Paleozoic basement in the NW Argentine Andes: *Zentralblatt für Geologie und Paläontologie, Teil I*, v. 1985, no. 9/10, p. 1245–1255.
- Willner, A.P., Miller, H., and Ježek, P., 1985, Geochemical features of an Upper Precambrian–Lower Cambrian greywacke/pelite sequence (Puncovicana trough) from the basement of the NW-Argentine Andes: Neues Jahrbuch für Geologie und Paläontologie, Monatshefte, v. 1985, p. 498–512.
- Willner, A.P., Lottner, U.S., and Miller, H., 1987, Early Paleozoic structural development in the NW Argentine basement of the Andes and its implication for geodynamic reconstructions, in McKenzie, G.D., ed., *Gondwana Six: Structure, Tectonics, and Geophysics: American Geophysical Union Geophysical Monograph 40*, p. 229–239.
- Zimmermann, U., 2005, Provenance studies of very low- to low-grade metasedimentary rocks of the Puncovicana complex, northwest Argentina, in Vaughan, A.P.M., Leat, P.T., and Pankhurst, R.J., eds., *Terrane Processes at the Margins of Gondwana: Geological Society of London Special Publication 246*, p. 381–416.

MANUSCRIPT RECEIVED 4 NOVEMBER 2013
 REVISED MANUSCRIPT RECEIVED 5 MARCH 2014
 MANUSCRIPT ACCEPTED 31 MARCH 2014

Printed in the USA

Table-TIMS-DR1: TIMS U-Pb geochronologic data and apparent ages (von Gosen et al.)

Sample CR-49D											
Sample	Pos-6	Pos-7 rc	Pos-8(1)	Pos-9 ic	Pos-10	Pos-11	Pos-6 ic	Pos-7	Pos-8(2)	Pos-9 rc	Pos-10 sl
no. of grains	2	1	1	1	1	1	1	1	1	1	1
ppm U	6172,85	1952.26	2824.92	3262.65	1432.36	4309.81	2691.02	1298.06	917.10	1993.27	1425.85
common Pb ppm	37,99	15.26	20.33	23.03	18.63	20.99	19.85	82.17	41.45	16.66	11.94
[206]nmoles/g	1510,48	544.496	515.325	950.62	397.19	1181.3	664.9	390.1	311.7	703.9	234.7
206/204	579,8	500.1	362.0	591.3	303.6	801.9	477.1	628.8	111.0	595.0	272.8
206/204 (corr.)	597,9	536.4	381.1	620.7	320.6	846.4	503.8	713.9	113.1	635.3	295.6
206*/238	0,0568956	0.0646179	0.0416634	0.0678242	0.0627366	0.0643149	0.0571187	0.0702359	0.0684472	0.0822652	0.0370468
207*/235	0,453841	0.465799	0.3354	0.57173	0.503113	0.511914	0.503293	0.560911	0.542554	0.636306	0.327455
207*/206*	0,0578528	0.0522811	0.0583857	0.0611371	0.0581626	0.0577277	0.0639059	0.0579206	0.0574892	0.0560981	0.0641063
206*/238 m.y.	356,7	403.6	263.1	423.0	392.2	401.8	358.1	437.6	426.8	509.6	234.5
207*/235 m.y.	380,0	388.3	293.7	459.1	413.8	419.7	413.9	452.1	440.1	500.0	287.6
207*/206* m.y.	524,2	297.7	544.3	644.1	535.9	519.4	738.5	526.8	510.3	456.3	745.1
206/204 %err	2,6	7.26	4.73	4.26	5.1	4.72	4.89	11.9	2.08	5.9	12.2
206*/238 %err	0,333	0.461	0.423	0.241	0.396	0.356	0.249	0.549	0.521	0.241	1.08
207*/235 %err	0,417	2.09	0.55	0.324	0.497	0.409	0.329	0.605	1.4	0.387	8.17
207*/206* %err	0,241	1.93	0.334	0.205	0.285	0.194	0.209	0.242	1.22	0.286	7.52
Rho	0,81635	0.4582	0.79523	0.77377	0.81929	0.88058	0.77406	0.916667	0.5062	0.67545	0.64464

Sample CE-54D

Sample	Pos-12 abr/ic	Pos-13 abr/ic	Pos-14 abr/ic	Pos-15 abr/ic	Pos-16 abr/ic	Pos-12	Pos-13	Pos-14	Pos-15	Pos-16
no. of grains	2	1	2	1	2	2	3	1	1	2
ppm U	4956.59	2258.06	4730.51	2348.52	5037,93	4087.85	11064	1817.26	1759.85	3464.2
common Pb ppm ppm	20.95	17.14	10.38	8.078	21,22	17.59	9,349	10.71	14.26	16.56
[206]nmoles/g	1705.59	906.18	1434.67	920.03	1574,32	1327.91	3812.33	669.42	618.34	1047.41
206/204	1158.6	744.9	1866.6	1496.5	1056,8	1064.05	5434.85	849.48	604.39	888.65
206/204 (corr.)	1224.4	794.9	2079.0	1712.6	1115,8	1135.15	6131.54	940.21	652.06	950,991
206*/238	0.0812864	0.0940314	0.0720838	0.0929359	0,073711	0.0766457	0.0823726	0.0866239	0.0819083	0.0711152
207*/235	0.695349	0.80397	0.605001	0.783533	0,569075	0.613693	0.65589	0.690041	0.653104	0.559718
207*/206*	0.0620417	0.0620105	0.060872	0.0611467	0,055993	0.0580714	0.0577493	0.0577745	0.0578299	0.0570829
206*/238 m.y.	503.8	579.3	448.7	572.9	458,5	476.1	510.3	535.5	507.5	442.9
207*/235 m.y.	536.0	599.1	480.4	587.5	457,4	485.9	512.1	532.8	510.4	451.3
207*/206* m.y.	675.5	674.5	634.7	644.4	452,1	532.5	520.3	521.2	523.3	494.7
206/204 %err	4.91	5.77	9.63	12.4	4,76	6.67	10.8	9.23	6.87	6.02
206*/238 %err	1.72	0.367	0.349	1.03	1,91	1	0.667	0.35	0.475	0.982
207*/235 %err	1.75	0.446	0.366	1.05	1,93	1.42	0.677	0.408	0.528	1.03
207*/206* %err	0.298	0.241	0.104	0.174	0,273	0.962	0.113	0.2	0.22	0.308
Rho	0.985402	0.84127	0.958495	0.986151	0,98995	0.73729	0.985907	0.87227	0.909628	0.954599

Sample CE-55D

Sample	Pos-6	Pos-7	Pos-8	Pos-10	Pos-11	Pos-12	Pos-13	Pos-14	Pos-15	Pos-16
no. of grains	1	1	2	3	1	1	1	1	1	1
ppm U	2163.48	2044.34	4549.89	5043.23	2463,38	1329.42	2301.71	1868.74	1059.83	1107.26
common Pb ppm	70.88	77.71	14.54	20.72	13,55	4614.00	6012.00	11.51	4468.00	5952.00
[206]nmoles/g	710.10	730.59	1518.39	1870.2	843,6	438.5	708.8	591.7	348.5	388.0
206/204	1294.9	1230.5	1452.1	1283.2	863,0	1144.8	1485.9	703.6	935.5	823.9
206/204 (corr.)	1506.4	1413.7	1570.2	1357.0	936,4	1429.1	1772.8	772747.0	1172.9	980154.0
206*/238	0.0777521	0.0845905	0.0790935	0.0877285	0,080525	0.0780781	0.0730858	0.0741465	0.0776237	0.082464
207*/235	0.606264	0.666655	0.625809	0.707356	0,640901	0.625825	0.582605	0.577407	0.623965	0.63858
207*/206*	0.056552	0.0571582	0.0573852	0.0584784	0,057724	0.0581329	0.0578149	0.0564794	0.0582995	0.0561629
206*/238 m.y.	482.7	523.5	490.7	542.1	499,3	484.6	454.7	461.1	481.9	510.8
207*/235 m.y.	481.2	518.7	493.5	543.2	502,9	493.5	466.1	462.8	492.3	501.4
207*/206* m.y.	474.1	497.6	506.4	547.7	519,3	534.8	522.8	471.3	541.0	458.8
206/204 %err	14.1	12.8	6.95	4.91	7,3	21.5	16.6	8.68	22.2	16.7
206*/238 %err	0.533	1.18	0.333	0.822	0,606	0.393	0.337	0.462	0.44	1.31
207*/235 %err	0.588	1.21	0.407	0.853	0,644	0.498	0.419	0.775	0.58	1.48
207*/206* %err	0.235	0.254	0.22	0.215	0,208	0.297	0.236	0.586	0.358	0.646
Rho	0.917041	0.977847	0.84193	0.967738	0,946442	0.80266	0.82603	0.65704	0.78804	0.89938

analytical errors are quoted at 1 sigma level

data point ellipses are 2 sigma

grey marked positions are excluded for concordia calculation: ic = inherited core, rc = reverse concordant, sl = strong Pb-loss, abr = abraded

calculated concordia data are quoted at 95% level

used programs: PBDAT vers. 1.24, July 30, 1993, and ISOPLOT vers. 3.50, June 21, 2006 with kind permission of K.J. Ludwig (Berkeley Geochronology Center)

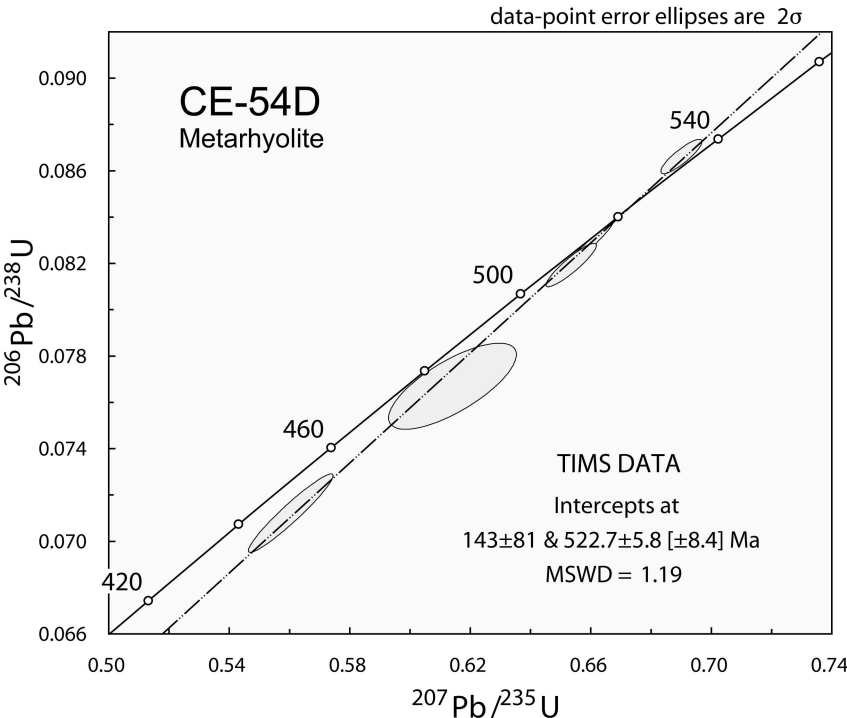


Figure-TIMS-DR1: Concordia diagram of single zircons (TIMS), sample CE-54D. Abraded zircons with cores are not used for the calculation (von Gosen et al.).

The TIMS analyses define a linear array indicating Pb-loss at about 145 Ma (lower intercept) and a crystallization age of 522.7 ± 5.8 [± 8.4] Ma (upper intercept). Abrasion of some grains clearly enhanced the presence of inherited cores. Analyses impacted by the presence of cores are not included in the regression and not plotted.

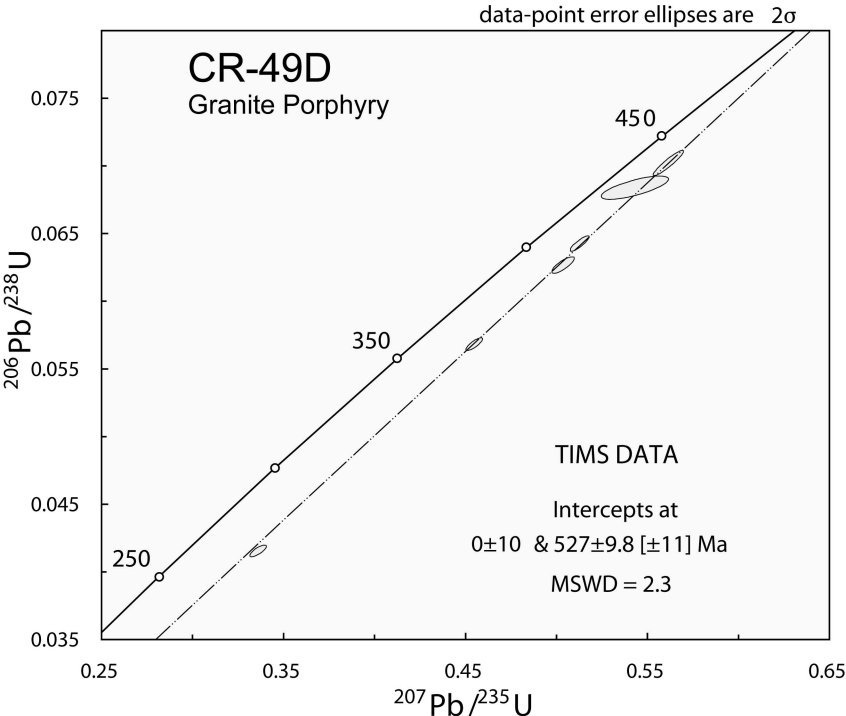


Figure-TIMS-DR2: Concordia diagram based on single zircons (TIMS), sample CR-49D (von Gosen et al.)

Excluding two reversely concordant analyses and one showing extreme Pb-loss and forcing a lower intercept of 0 ± 10 Ma, the remaining analyses define a Pb-loss cord with an upper intercept of $527 \pm 9.8 [\pm 11]$ Ma.

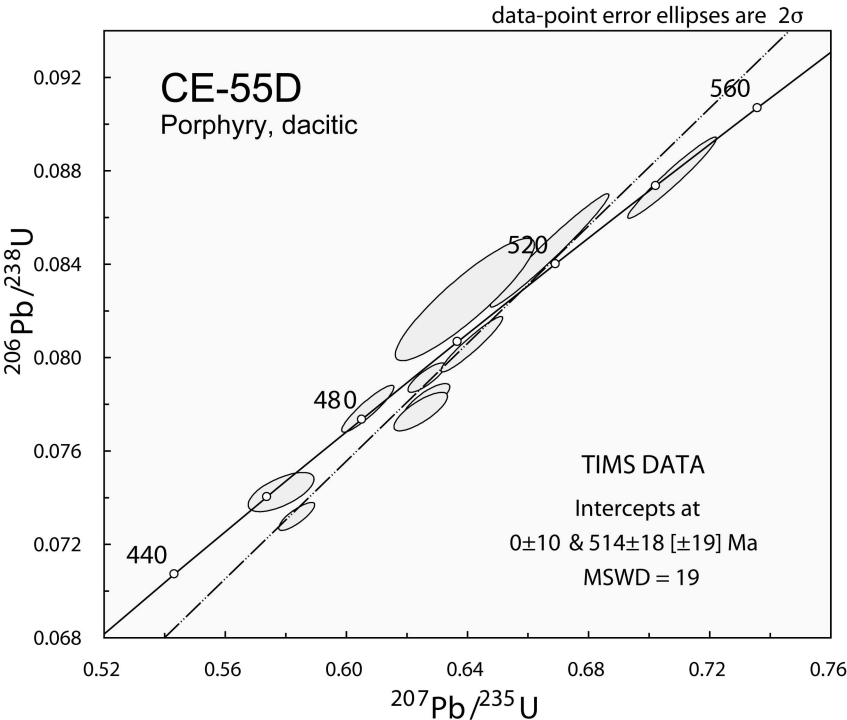


Figure-TIMS-DR3: Concordia diagram based on single zircons (TIMS), sample CE-55D (von Gosen et al.)

Concordant to discordant single grain TIMS analyses show considerable scatter ranging from 460 to 540 Ma and defining a linear array with an upper intercept of 514 ± 18 [± 19] Ma.